Supporting Information For

Molecular insights into the effects of Representative Organic Molecules on Spontaneous Hydrate Nucleation in Oceanic Sediments

Fengyi Mi[a,b], Zhongjin He[*,a], Jiangtao Pang[a], Othonas A. Moultos[c], Thijs J.H. Vlugt[c], Guosheng Jiang[a], Fulong Ning[a]

[a]National Center for International Research on Deep Earth Drilling and Resource Development, Faculty of Engineering, China University of Geosciences, Wuhan, Hubei 430074, China

[b]Key Laboratory of Solid Waste Treatment and Resource Reuse, Ministry of Education, Southwest University of Science and Technology, Mianyang 621010, Sichuan, China

[c]Engineering Thermodynamics, Process & Energy Department, Faculty of Mechanical Engineering, Delft University of Technology, Leeghwaterstraat 39, Delft, 2628CB, the Netherlands

[*]Authors to whom correspondence should be addressed. hezhongjin@cug.edu.cn

Total number of pages: 32

Total number of figures: 26

Total number of tables: 3

Total number of videos: 7

Contents of Supporting Information

S1. Simulation details S4

S1.1 Additional simulation models S4

Fig. S1. The molecular structures of the six small organic molecules *i.e.,* butane, propanol, phenylpropane, pentene, butyric-acid, and propylamine, used in this study S4

Table S1. The parameters for the seven systems of the slit-nanopore models S5

Table S2. The force field parameters for H_2O, CH_4, and clay S5

Table S3. The force field parameters for six organic molecules S6

S1.2 Additional simulation methods S7

S2. Calculation of properties **S8**

S2.1. Calculation principle of the diffusion coefficient (KDC) S8

S2.2. Calculation principle of the residence time correlation function S8

S2.3. Calculation principles of the distance between hydrate and nanobubbles (HBD) S8

S2.4. Calculation principle of the average hydrate formation ratio (RHF) S9

S3. Additional information for Results and Discussions **S10**

Fig. S2. Number density distribution of H_2O molecules over the last 0.001 μs in the seven systems S10

Fig. S3. Number density distribution of ions over the last 0.001 μs in the seven systems S11

Fig. S4. Number density distribution of CH_4 molecules over the last 0.001 μs in the seven systems S12

Fig. S5. Number density distribution of H_2O, CH_4, organic molecules and ions along the surface normal direction (z-axis) over the 2.5 - 3.0 μs in the seven system S13

Fig. S6. Number density distribution of small organic molecules over the last 0.001 μs in the six systems S13

Fig. S7. Radial distribution function g(r) of organic molecules and other atoms (Na^+, Cl^-, water oxygen atoms and methane carbon atoms) during the simulation period of 0.001 - 0.005 μs in the six organic molecules S14

Fig. S8. Evolution of the average residence time (τ_{Res}) for ions, H_2O and CH_4 near the organic molecules in the six systems S15

Fig. S9. Aggregation processes of CH_4 nanobubbles for the y-x plane in the (a-d) $MO_{Propanol}$ system S16

Fig. S10. Snapshots of CH_4 hydrates formed at the end of the simulation (at the 3.0 μs) for the y-x plane in the different simulations S17

Fig. S11. Evolution of the number of CH_4 in nanobubble, dissolved solution and near the organic molecules in the seven systems S18

Fig. S12. Evolution of the diffusion coefficient (k_{DC}) for three types of CH_4 molecules during the hydrate formation in the seven system S19

Fig. S13. Evolution of the number of three types of H_2O molecules in the seven systems S20

Fig. S14. Evolution of the diffusion coefficient (k_{DC}) for three types of H_2O molecules during the hydrate formation in the seven systems. S21

Fig. S15. Evolution of the number of (a) H_2O and (b) CH_4 molecules near organic molecules in the six systems S21

Fig. S16. Evolution of (a) CH_4 mole fraction in water (x_{CH4}) for solutions and (b) the number of CH_4 molecules in the nanobubbles (N_{CH4}) for the seven systems S22

Fig. S17. (a) Schematic representation of the interface region and bulk solution in the simulation box. Evolution of CH_4 mole fraction in water (x_{CH4}) for (b) interfacial region and (c) bulk solution in the seven systems S22

Fig. S18. Probability distribution of the distance between CH_4 in hydrate and nanobubbles (HBD) over the last 0.05 μs in the seven systems S23

Fig. S19. Probability distribution of the distance between H_2O in hydrate and nanobubbles (HBD) over the last 0.05 μs in the seven systems S24

Fig. S20. Evolution of the number of CH_4 molecules in hydrate cages under the distance between hydrate and nanobubbles (HBD) in the seven systems S25

Fig. S21. Evolution of the number of H_2O molecules in hydrate cages under the distance between hydrate and nanobubbles (HBD) in the seven systems S26

Fig. S22. Evolution of the number of hydrate cages for the seven systems S27

Fig. S23. Evolution of F_4 near the organic molecules in the six systems S27

Fig. S24. Snapshots of the (a) complete cage and (b) cage-like hydrogen-bond networks of water molecules near the butane molecule in the MO_{Butane} system. (c) Snapshots of cage-like structures on the surface of butane adsorbed on nanobubble surface S28

Fig. S25. Evolution of the number of hydrate cages in the seven system S29

Fig. S26. Evolution of crystallinity ($5^{12}6^2/5^{12}$) for the seven systems S29

S4. Supporting Videos **S30**

Video S1. Spontaneous nucleation processes of CH_4 hydrates in the $MO_{No\text{-}organic}$ system S30

Video S2. Spontaneous nucleation processes of CH_4 hydrates in the $MO_{Butyric\text{-}acid}$ system S30

Video S3. Spontaneous nucleation processes of CH_4 hydrates in the $MO_{Propylamine}$ system S30

Video S4. Spontaneous nucleation processes of CH_4 hydrates in the $MO_{Propanol}$ system S30

Video S5. Spontaneous nucleation processes of CH_4 hydrates in the $MO_{Pentene}$ system S30

Video S6. Spontaneous nucleation processes of CH_4 hydrates in the MO_{Butane} system S31

Video S7. Spontaneous nucleation processes of CH_4 hydrates in the $MO_{Phenylpropane}$ system S31

References **S31**

S1. Simulation details

S1.1 Additional simulation Models

A homogeneous solution containing 5352 H_2O molecules and 931 CH_4 molecules was placed in the montmorillonite nanopores. This gas-water ratio is in line with the standard SI-type hydrate, enabling the potential formation of CH_4 hydrates involving all H_2O and CH_4 molecules. Sodium chloride with a salinity of 3.5 wt% was randomly placed into the homogeneous solution, which is closer to the real ocean environment. We selected six different small organic molecules, named butane, propanol, phenylpropane, pentene, butyric-acid, and propylamine. They have the same propyl skeleton and different functional groups methyl, hydroxyl, phenyl, double bond, carboxyl and amino (Fig. S1). These six functional groups are commonly found in the ocean. All organic molecules are represented using the OPLS-AA force field. The numbers of CH_4, H_2O and ions in the seven systems are all consistent (Table S1), and they are all randomly inserted into the nanopores. 50 organic molecules were added to the solution. Too high a concentration may greatly hinder the spontaneous nucleation of CH_4 hydrate, while too low a concentration cannot show the effect of organic molecules on the spontaneous nucleation of CH_4 hydrate. The detailed force field parameters for H_2O, CH_4, ions, montmorillonite, and organic molecules in the system are shown in Table S2 and Table S3.

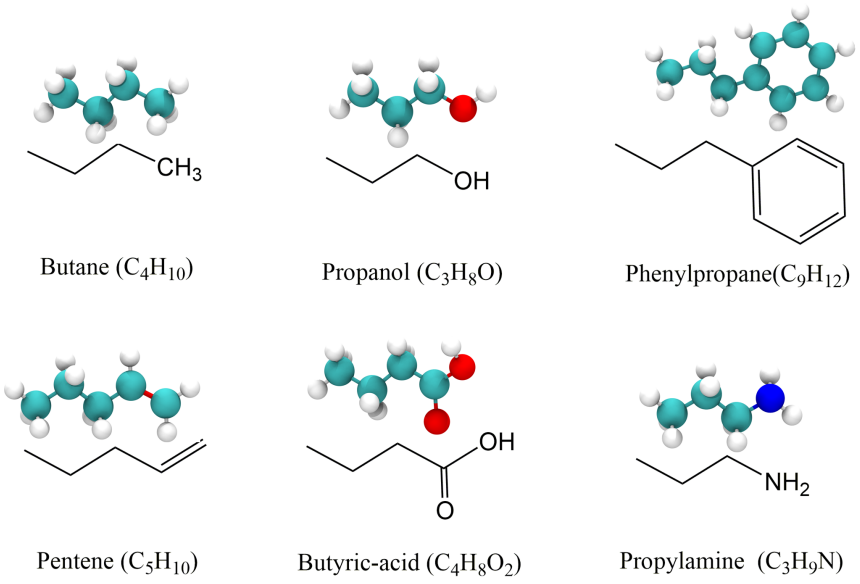


Fig. S1. The molecular structures of the six small organic molecules *i.e.,* butane, propanol, phenylpropane, pentene, butyric-acid, and propylamine, used in this study.

Table S1. The parameters for the seven systems of the slit-nanopore models.

	Systems: 250 K/50 MPa/0 - 3.0 μs simulation time				
System	N_{CH4}	N_{H2O}	N_{Na+}	N_{Cl-}	$N_{organic}$
$MO_{No\text{-}organic}$	931	5352	240	60	50
$MO_{Butyric\text{-}acid}$	931	5352	240	60	50
$MO_{Propylamine}$	931	5352	240	60	50
$MO_{Propanol}$	931	5352	240	60	50
$MO_{Pentene}$	931	5352	240	60	50
MO_{Butane}	931	5352	240	60	50
$MO_{Phenylpropane}$	931	5352	240	60	50

Table S2. Parameters for the TIP4P/ice water model (Abascal et al., 2005), OPLS-UA methane (Jorgensen et al., 1984), and the CLAYFF force field (Cygan et al., 2004). σ and ε are the Lennard-Jones parameters, in units of nm and kJ/mol, respectively; q is the partial charge of an atom in units of elementary charge (e); m is the atomic mass in units of g/mol.

atom	ε, kJ/mol	σ, nm	q, e	m, g/mol
H_2O				
O (MW)	0	0	-1.1794	0
O	0.8822	0.31668	0	16
H	0	0	0.5897	1.008
CH_4	1.23	0.373	0	16
Ion				
Cl	0.418998	0.439997	-1	35.453
Na	0.544572	0.235002	1	22.989
Montmorillonite				
Si (st)	7.70065×10^{-6}	0.3302	2.1	28.09
Al (ao)	5.56388×10^{-6}	0.4271	1.575	26.98
Mg (mgo)	3.77807×10^{-6}	0.5264	1.3598	24.31
O (ob)	0.65017	0.316556	-1.05	16
O (obts)	0.65017	0.316556	-1.1688	16
O (obos)	0.65017	0.316556	-1.1808	16
O (oh)	0.65017	0.316556	-0.95	16
O (ohs)	0.65017	0.316556	-1.0808	16
H (ho)	0	0	0.425	1.008

Table S3. Parameters for the OPLS-AA force field (Jorgensen et al., 1996) for the six organic molecules. σ and ε are the Lennard-Jones parameters, in units of nm and kJ/mol, respectively; q is the partial charge of an atom in units of elementary charge (e); m is the atomic mass in units of g/mol.

atom	ε, kJ/mol	σ, nm	q, e	m, g/mol
Butyric-acid				
C(C)	0.43932	0.375	0.52	12.011
C(CT)	0.276144	0.35	-0.12	12.011
C(CT1)	0.276144	0.35	-0.18	12.011
O (O3)	0.87864	0.296	-0.44	15.999
O (OH)	0.71128	0.3	-0.53	15.999
H (HO)	0	0	-0.45	1.008
H (HC)	0.12552	0.25	0.06	1.008
Propylamine				
C(CT)	0.276144	0.35	-0.06	12.011
C(CT1)	0.276144	0.35	-0.12	12.011
C(CT2)	0.276144	0.35	-0.18	12.011
N (NT)	0.71128	0.33	-0.9	14.007
H (H)	0	0	0.36	1.008
H (HC)	0.12552	0.25	0.06	1.008
Propanol				
C(CT)	0.276144	0.35	0.145	12.011
C(CT1)	0.276144	0.35	-0.12	12.011
C(CT2)	0.276144	0.35	-0.18	12.011
O (OH)	0.71128	0.312	-0.683	15.999
H (HO)	0	0	0.418	1.008
H (HC)	0.12552	0.25	0.06	1.008
Pentene				
C(C)	0.317984	0.355	-0.23	12.011
C(CT)	0.276144	0.35	-0.12	12.011
C(CT1)	0.276144	0.35	-0.18	12.011
C(CT2)	0.317984	0.355	-0.115	12.011
H (HT)	0.12552	0.25	0.115	1.008
H (HC)	0.12552	0.25	0.06	1.008
Butane				
C(CT)	0.276144	0.35	-0.12	12.011
C(CT1)	0.276144	0.35	-0.18	12.011
H (HC)	0.12552	0.25	0.06	1.008
Phenylpropane				
C(CA)	0.29288	0.355	-0.115	12.011
C(CT)	0.276144	0.35	-0.12	12.011
C(CT1)	0.276144	0.35	-0.005	12.011
C(CT1)	0.276144	0.35	-0.18	12.011
H (HA)	0.12552	0.242	0.115	1.008
H (HC)	0.12552	0.25	0.06	1.008

Additional simulation methods

Montmorillonite and pyrophyllite are both 2:1 type clay minerals with similar structures. Pyrophyllite is electrically neutral, montmorillonite carries an electronegative charge. In this study, we conducted an isomorphic substitution of the pyrophyllite unit cell sourced from the American Mineral Crystal Database to transform it into an electronegative montmorillonite unit cell (Downs and Hall-Wallace, 2003). Initial crystal was substitutions, replacing Al^{3+} with Mg^{2+} in the octahedral sheets and Si^{4+} with Al^{3+} in the tetrahedral sheets, conforming to Loewenstein's rule (Loewenstein, 1954). Subsequently, a montmorillonite slab was obtained by expanding the cell along the xy direction (12×10). The montmorillonite nanopore was created by stacking two identical montmorillonite slabs with a defined pore size of 4.0 nm. The final model consists of a slit nanopore and a homogeneous solution. The size of the simulation box was 6.19 × 15.36 × 5.39 nm^3. We selected the Wyoming montmorillonite model due to the universality and usability of the model. Wyoming montmorillonite is a widely studied and described type of montmorillonite. In previous studies on the formation and decomposition of gas hydrate in montmorillonite nanopores, the Wyoming montmorillonite model has always been adopted (Li et al., 2022; Mi et al., 2022). To enhance the CH_4 hydrate formation rate and minimize computational costs, production simulations were conducted under the conditions of temperature 250 K and pressure 50 MPa. The nucleation of hydrates takes a long time. Under the extreme conditions of 250 K and 50 MPa, it also takes a long time to observe the occurrence of hydrate nucleation events. Therefore, in this study, we performed long-term microsecond molecular simulations to investigate hydrate nucleation and growth. But at the end of our 2 μs simulation, there are still a large number of CH_4 molecules and H_2O molecules that have not been converted into hydrates.

The equilibration simulation was conducted at 250 K and 50 MPa, with the pressure and temperature controlled by Berendsen barostat (Berendsen et al., 1984) (time constant 1.0 ps) and velocity-rescaling thermostat (Bussi et al., 2007) (time constant 0.1 ps), respectively. For the production runs, each system was performed at 250 K and 50 MPa, and the pressure and temperature were regulated by the Parrinello-Rahman barostat (Parrinello and Rahman, 1980) and Nosé-Hoover thermostat (Nose, 1984) with the corresponding time constants of 4.0 and 2.0 ps, respectively. The pressure coupling was semi-isotropic, allowing independent fluctuations along the normal (z-dimension) and lateral (xy-dimensions) directions. There is a montmorillonite solid in the xy direction, so the length of the simulation box in the z direction is mainly controlled to achieve a pressure of 50 MPa. The F_4 order parameter serves as an effective discriminator for distinguishing the water phase, with average values of -0.04, -0.4, and 0.7 for liquid water, ice, and hydrate, respectively (Báez and Clancy, 1994). To monitor the growth of CO_2 hydrate in the different nanopores, the cage analysis algorithm proposed by Jacobson *et al.* (Jacobson et al., 2009) is used to display the seven cage types (5^{12}, $5^{12}6^2$, $5^{12}6^3$, $5^{12}6^4$, $4^15^{10}6^2$, $4^15^{10}6^3$, and $4^15^{10}6^4$).

S2. Calculation of properties

S2.1. Calculation principle of the diffusion coefficient (K_{DC})

The mean square displacement (MSD) and diffusion coefficient K_{DC} are calculated by the program *gmx_mpi msd* in GROMACS manual 5.0.7. Normally an index file containing atom numbers is used and the MSD is averaged over these atoms. For organic molecules consisting of more than one atom, r_i can be taken as the center of mass position of the organic molecules.

$$K_{DC} = \frac{\lim_{t\to\infty}\langle \|r_i(t) - r_i(0)\|^2 \rangle_{i\in A}}{6\Delta t} \quad (1)$$

In this study, each MSD is calculated within 1 ns for organic molecules and water molecules. Therefore, each diffusion coefficient is the average value within each 1 ns period.

S2.2. Calculation principle of the residence time correlation function

The principle of correlation functions is well established and documented in GROMACS manual 5.0.7. The residence time correlation function is one such function. The definition of the residence correlation function $C_f(t)$ for residence $f(t)$ is:

$$C_f(t) = \langle f(\xi) f(\xi + t) \rangle_\xi \quad (2)$$

$\langle\ \rangle$ indicates averaging over ξ, that is over time origins.

The residence time τ is calculated by the numeric integration of the residence correlation function:

$$\tau = \int_0^\infty C_f(t)dt \quad (3)$$

In practical MD simulation, correlation functions are calculated based on data points with discrete time intervals Δt, so the residence correlation function $C_f(t)$ is:

$$C_f(j\Delta t) = \frac{1}{N-j}\sum_{i=0}^{N-1-j} f(i\Delta t) f((i+j)\Delta t) \quad (4)$$

Where N is the number of available time frames for the calculation.

In this study, each τ_{Res} is calculated within 1 ns for CH_4, H_2O, and ions near small organic molecules. The GROMACS command *gmx_mpi hbond -ac -contact* can perform the calculation of the residence correlation function.

S2.3. Calculation principles of the distance between hydrate and nanobubbles (HBD)

To reveal the positional relationship between hydrate solids and CH_4 nanobubbles, we define a parameter HBD, which is the distance between hydrates (comprising CH_4 and H_2O molecules) and nanobubbles. CH_4 hydrate is

composed of CH_4 and H_2O molecules. We first select each CH_4 molecule or H_2O molecule that forms a hydrate and then calculate the distance between each CH_4 molecule in the nanobubble and the hydrate (the CH_4 molecule or H_2O molecule). The minimum value is the distance between the CH_4 molecules or H_2O molecules in the hydrate and the nanobubbles.

$$HBD \in \{D_1, D_2, D_3, D_4 \cdots\}_{min} \quad (5)$$

Where D_1 is the distance between the CH_4 or H_2O molecule and a CH_4 molecule in the nanobubbles. D_2 is the distance between the CH_4 or H_2O molecule and another CH_4 molecule in the nanobubbles. We count all distance values and only take the minimum value.

S2.4. Calculation principle of the average hydrate formation ratio (R_{HF})

To assess the stability of spontaneous nucleation of CH_4 hydrates in different HBD values, we define the hydrate formation ratio (R_{HF}). This metric gauges whether a hydrate (comprising CH_4 and H_2O molecules) will maintain its hydrate state or transition into another state for subsequent simulations. CH_4 hydrate is composed of CH_4 and H_2O molecules. R_{HF} is defined as the time during which the CH_4 or H_2O molecule retains its hydrate state in subsequent simulations divided by the total subsequent time.

$$R_{HF} = \frac{t_{Hydrate}}{t_{total}} \quad (6)$$

Where $t_{Hydrate}$ is the time during of the CH_4 or H_2O molecule retains its hydrate state. t_{total} is the time during the subsequent simulations. In this study, R_{HF} of CH_4 and H_2O molecules in hydrate cages under the HBD ranges (0 - 3.0 nm) for the six systems at 2.0 μs. Therefore, The CH_4 and H_2O molecules in the hydrate at time 2.0 μs will be labeled. $t_{Hydrate}$ is the time during of these CH_4 or H_2O molecules retain their hydrate state during 2.0 - 3.0 μs. t_{total} is the 1.0 μs for the time during of the subsequent simulations.

S3. Additional information for Results and Discussions

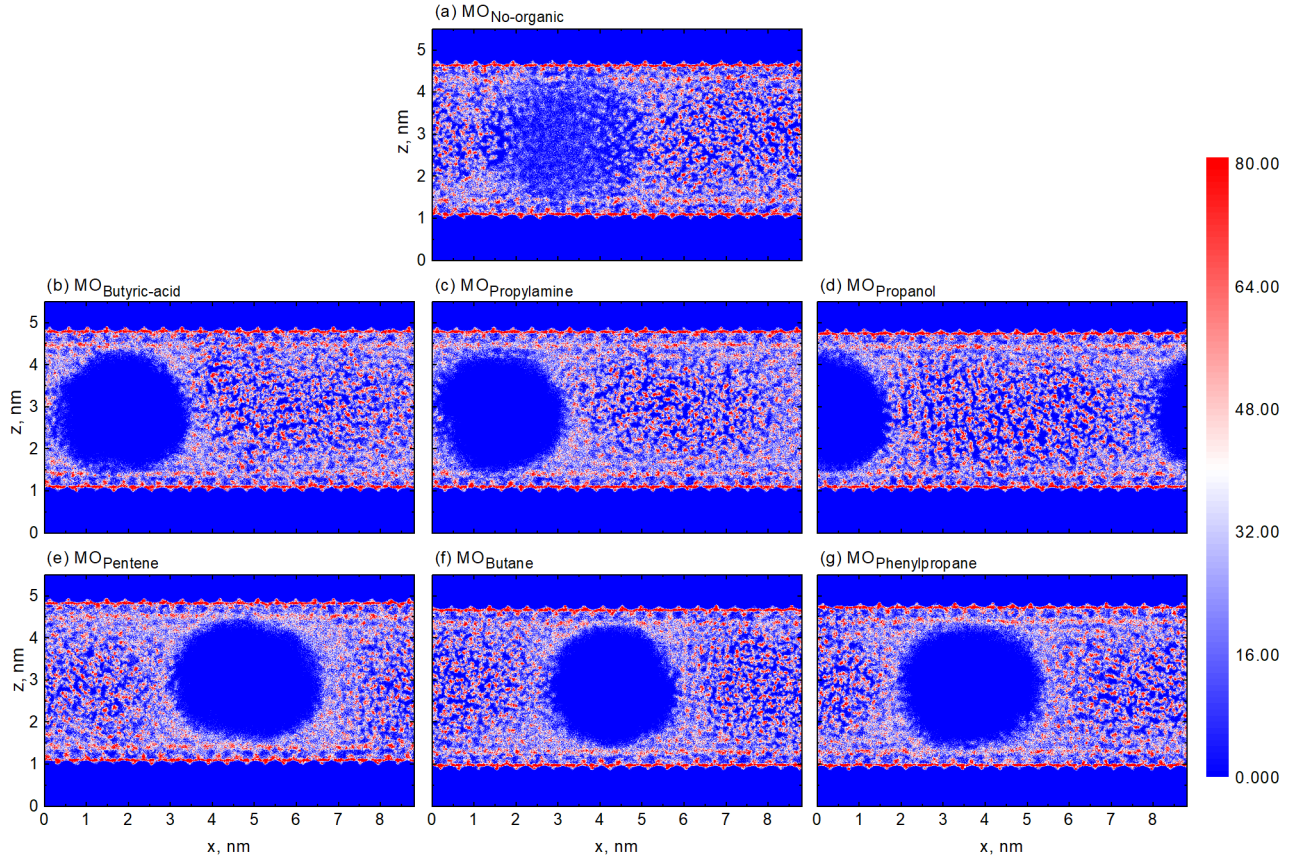


Fig. S2. Number density distribution of H_2O molecules over the last 0.001 μs in the seven systems *i.e.,* **(a)** $MO_{No\text{-}organic}$, **(b)** $MO_{Butyric\text{-}acid}$, **(c)** $MO_{Propylamine}$, **(d)** $MO_{Propanol}$, **(e)** $MO_{Pentene}$, **(f)** MO_{Butane} and **(g)** $MO_{Phenylpropane}$.

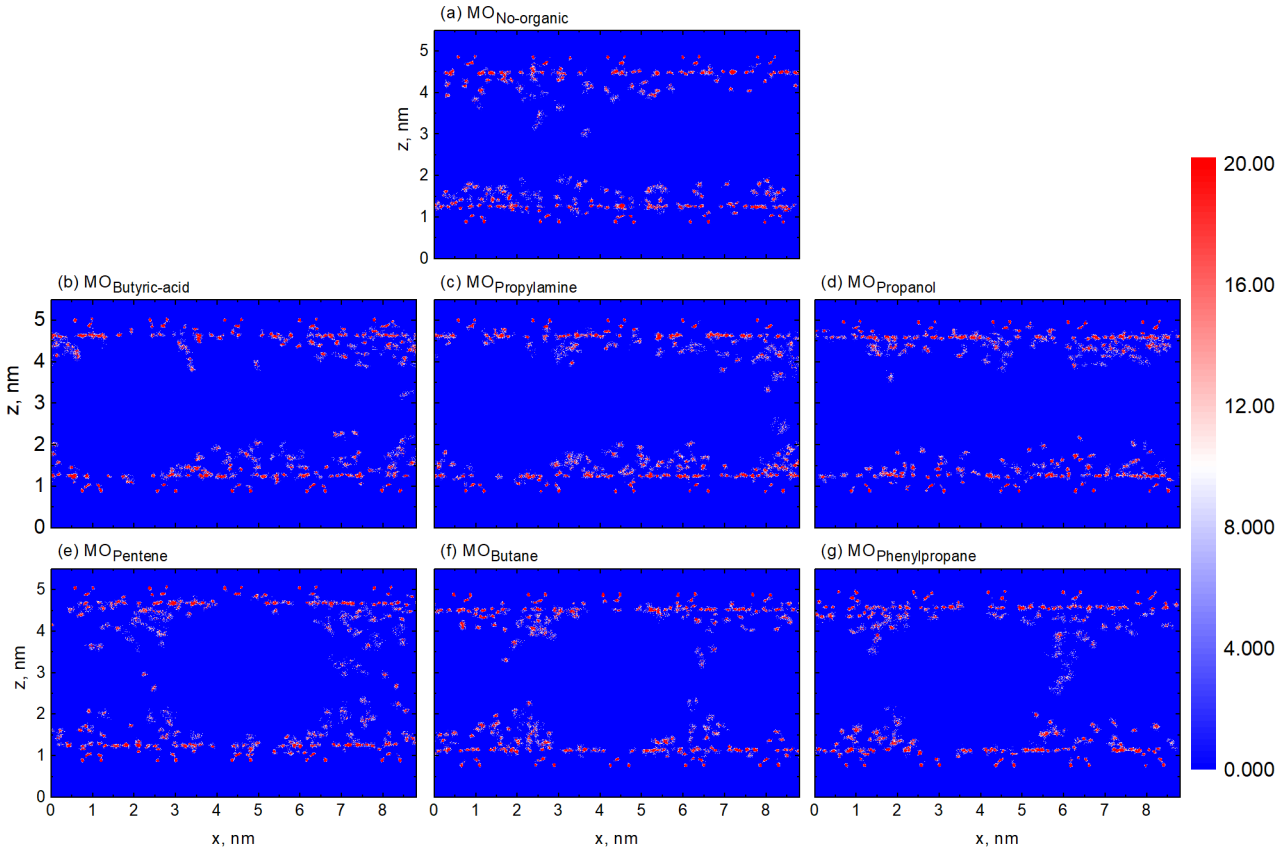


Fig. S3. Number density distribution of ions over the last 0.001 μs in the seven systems *i.e.,* **(a)** $MO_{No\text{-}organic}$, **(b)** $MO_{Butyric\text{-}acid}$, **(c)** $MO_{Propylamine}$, **(d)** $MO_{Propanol}$, **(e)** $MO_{Pentene}$, **(f)** MO_{Butane} and **(g)** $MO_{Phenylpropane}$.

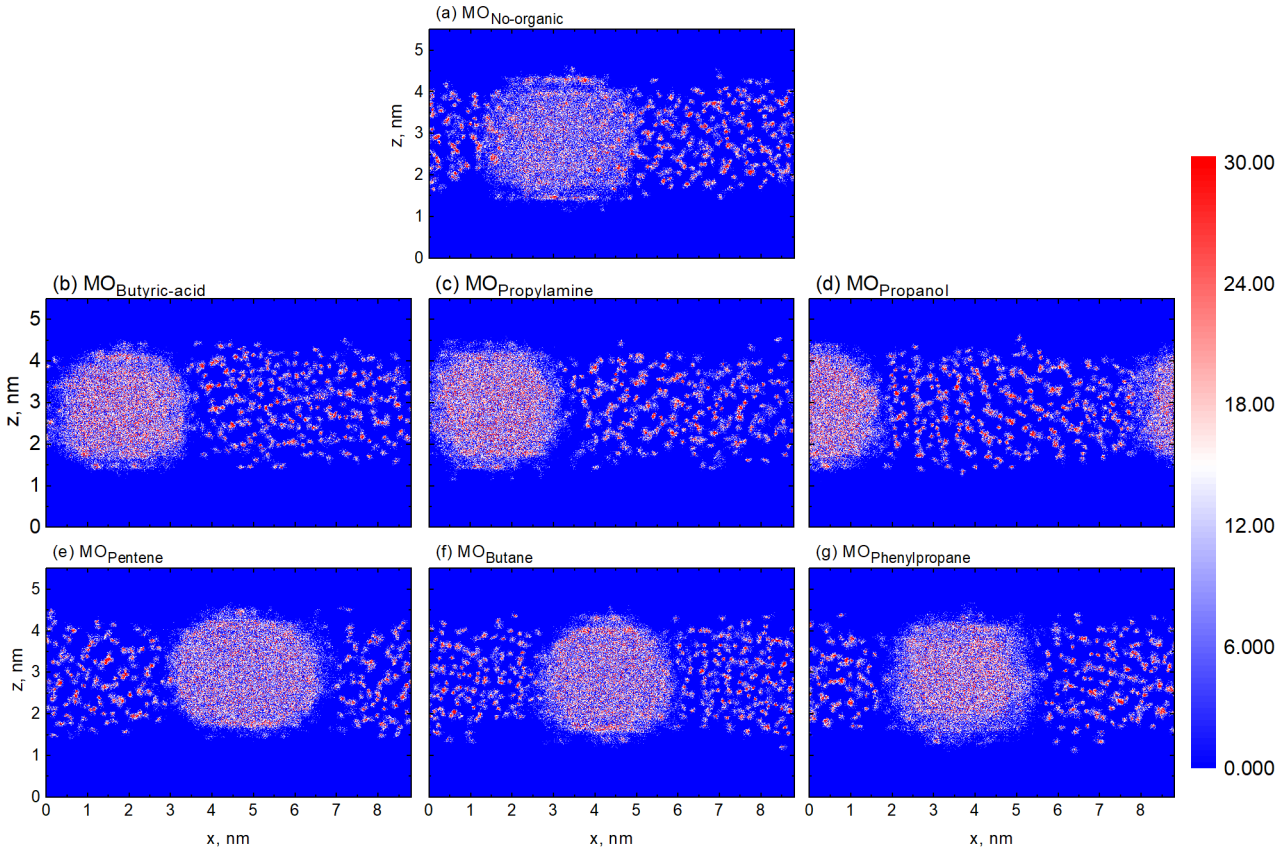


Fig. S4. Number density distribution of CH_4 molecules over the last 0.001 μs in the seven systems *i.e.,* **(a)** $MO_{No\text{-}organic}$, **(b)** $MO_{Butyric\text{-}acid}$, **(c)** $MO_{Propylamine}$, **(d)** $MO_{Propanol}$, **(e)** $MO_{Pentene}$, **(f)** MO_{Butane} and **(g)** $MO_{Phenylpropane}$.

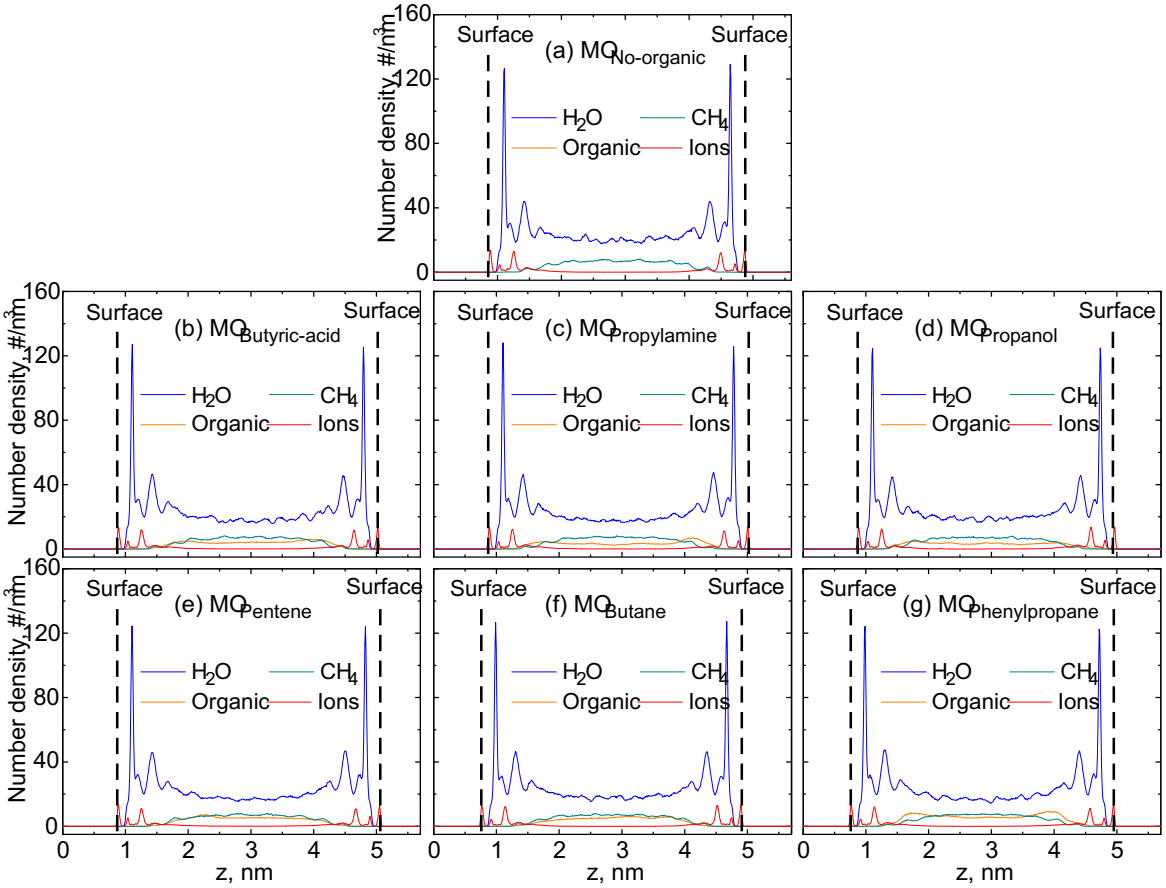


Fig. S5. Number density distribution of H_2O, CH_4, organic molecules and ions along the surface normal direction (z-axis) over the 2.5 - 3.0 μs in the seven systems *i.e.,* **(a)** $MO_{No\text{-}organic}$, **(b)** $MO_{Butyric\text{-}acid}$, **(c)** $MO_{Propylamine}$, **(d)** $MO_{Propanol}$, **(e)** $MO_{Pentene}$, **(f)** MO_{Butane} and **(g)** $MO_{Phenylpropane}$.

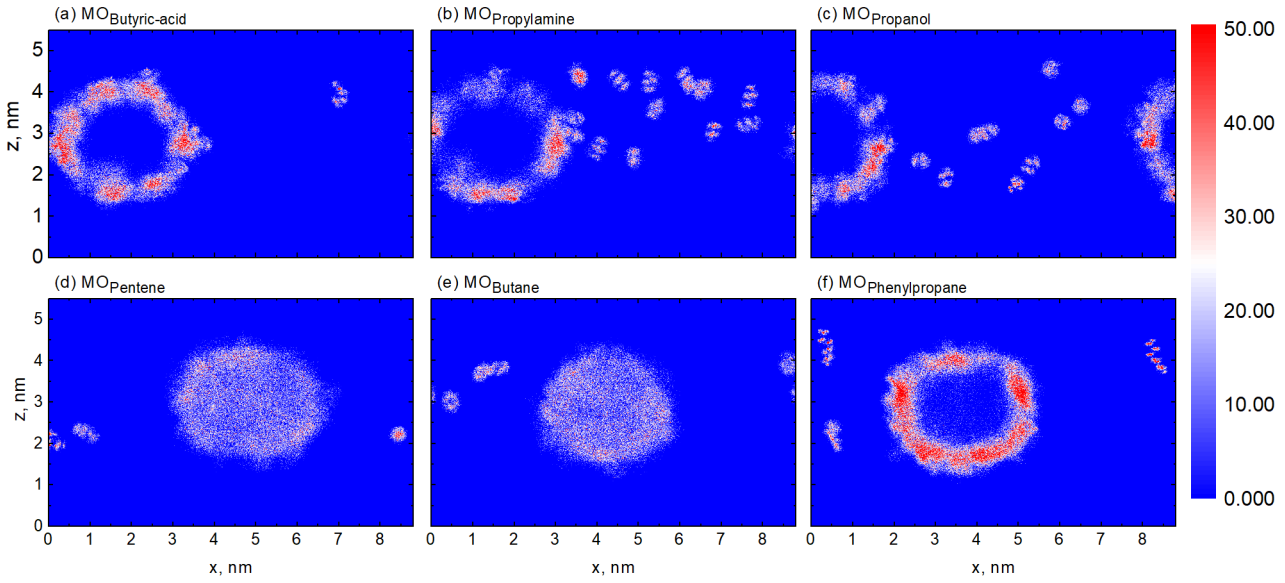


Fig. S6. Number density distribution of small organic molecules over the last 0.001 μs in the six systems *i.e.,* **(a)** $MO_{Butyric\text{-}acid}$, **(b)** $MO_{Propylamine}$, **(c)** $MO_{Propanol}$, **(d)** $MO_{Pentene}$, **(e)** MO_{Butane}, and **(f)** $MO_{Phenylpropane}$.

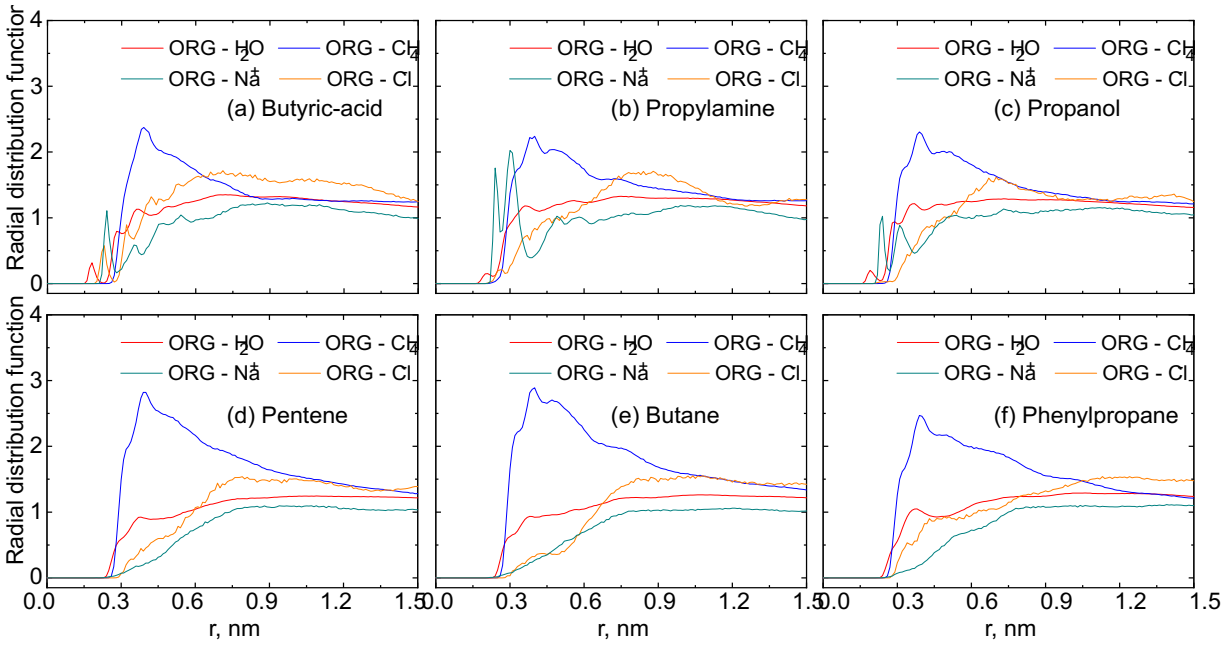


Fig. S7. Radial distribution function g(r) of organic molecules and other atoms (Na^+, Cl^-, water oxygen atoms and methane carbon atoms) during the simulation period of 0.001 - 0.005 μs in the six organic molecules *i.e.,* **(a)** Butyric-acid, **(b)** Propylamine, **(c)** Propanol, **(d)** Pentene, **(e)** Butane, and **(f)** Phenylpropane.

In the early stage of simulation, the radial distribution functions (RDF) of CH_4, H_2O, Na^+ and Cl^- ions around different organic molecules are shown in Fig. S7(a)–(f). It is found that the RDF of six organic molecules to CH_4 has a peak, indicating that there are CH_4 molecules near the organic molecules (Fig. S7(a)–(f)). In addition, the RDF of Na^+ ions exhibits obvious first peaks in butyric-acid, propylamine and propanol molecules but not in other organic molecules, which indicates that Na^+ ions can be enriched near butyric-acid, propylamine and propanol molecules (Fig. S7(a)–(f)). This is attributed to the fact that hydrophilic functional groups can attract Na^+ ions. Although the hydrophilic functional group can form hydrogen bonds with H_2O molecules in the solution to inhibit hydrate formation, it can attract salt ions, thereby inhibiting the fluctuation of salt ions and favoring hydrate formation. In contrast, the RDF of H_2O molecules and Cl^- ions have no obvious peaks (Fig. S7(a)–(f)). A cutoff radius of 0.4 nm is adopted to describe CH_4, H_2O and ions near the six organic molecules.

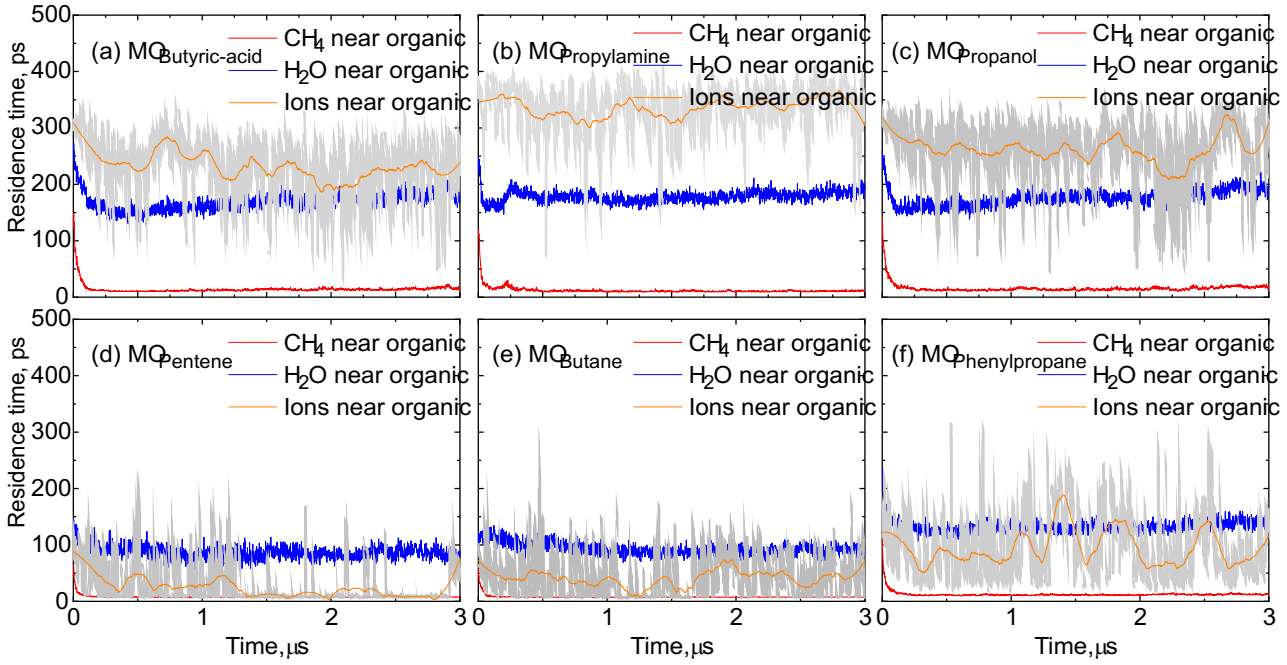


Fig. S8. Evolution of the average residence time (τ_{Res}) for ions, H_2O and CH_4 near the organic molecules in the six systems *i.e.,* **(a)** $MO_{Butyric\text{-}acid}$, **(b)** $MO_{Propylamine}$, **(c)** $MO_{Propanol}$, **(d)** $MO_{Pentene}$, **(e)** MO_{Butane} and **(f)** $MO_{Phenylpropane}$. These τ_{Res} were calculated for each ns.

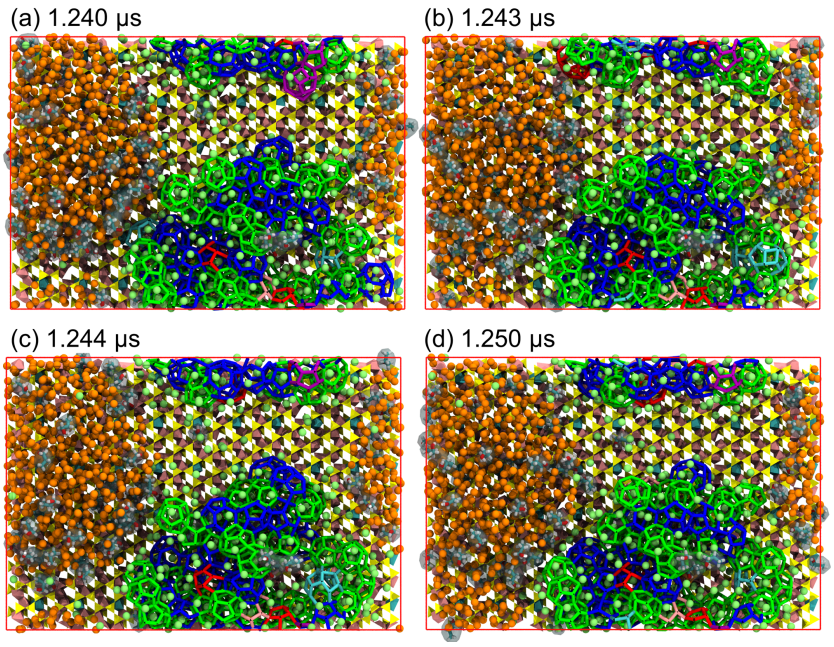


Fig. S9. Aggregation processes of CH_4 nanobubbles for the y-x plane in the **(a-d)** $MO_{Propanol}$ system. Small organic molecules are displayed as cyan (C atom), red (O atom) blue (N atom) and white (H atom). Clay layers are displayed as polyhedral, *i.e.,* yellow (Si atom), cyan (Mg atom) and pink (Al atom). Orange and green balls represent CH_4 in nanobubble and solution, respectively. Hydrate cages are shown as sticks in various colors (green for 5^{12}, blue for $5^{12}6^2$, red for $5^{12}6^3$, orange for $5^{12}6^4$, cyan for $4^15^{10}6^2$, purple for $4^15^{10}6^3$ and pink for $4^15^{10}6^4$).

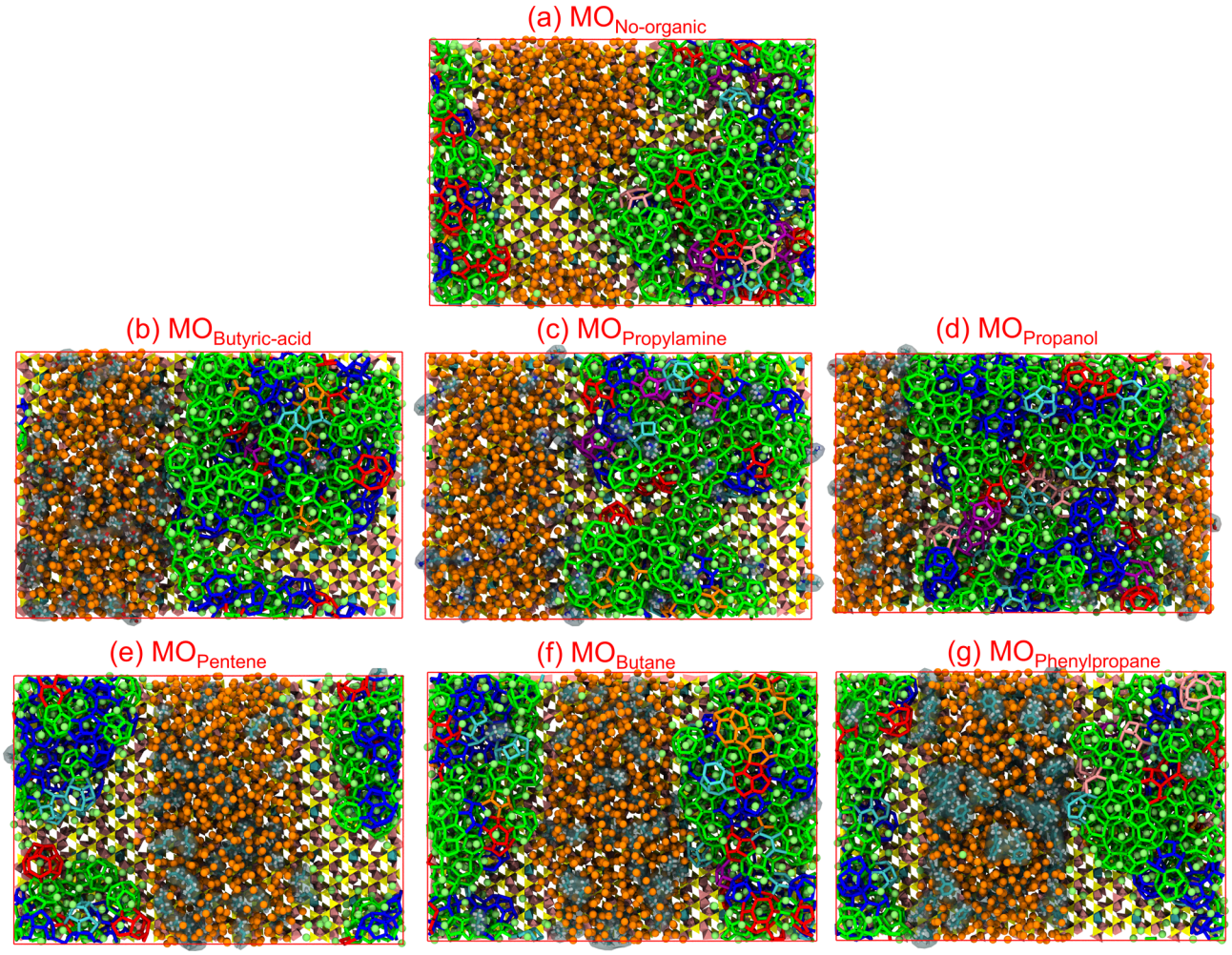


Fig. S10. Snapshots of CH_4 hydrates formed at the end of the simulation (at the 3.0 μs) for the y-x plane in the different simulations: **(a)** $MO_{No\text{-}organic}$, **(b)** $MO_{Butyric\text{-}acid}$, **(c)** $MO_{Propylamine}$, **(d)** $MO_{Propanol}$, **(e)** $MO_{Pentene}$, **(f)** MO_{Butane} and **(g)** $MO_{Phenylpropane}$. Small organic molecules are displayed as cyan (C atom), red (O atom) blue (N atom) and white (H atom). Clay layers are displayed as polyhedral, *i.e.,* yellow (Si atom), cyan (Mg atom) and pink (Al atom). Orange and green balls represent CH_4 in nanobubble and solution, respectively. Hydrate cages are shown as sticks in various colors (green for 5^{12}, blue for $5^{12}6^2$, red for $5^{12}6^3$, orange for $5^{12}6^4$, cyan for $4^15^{10}6^2$, purple for $4^15^{10}6^3$ and pink for $4^15^{10}6^4$).

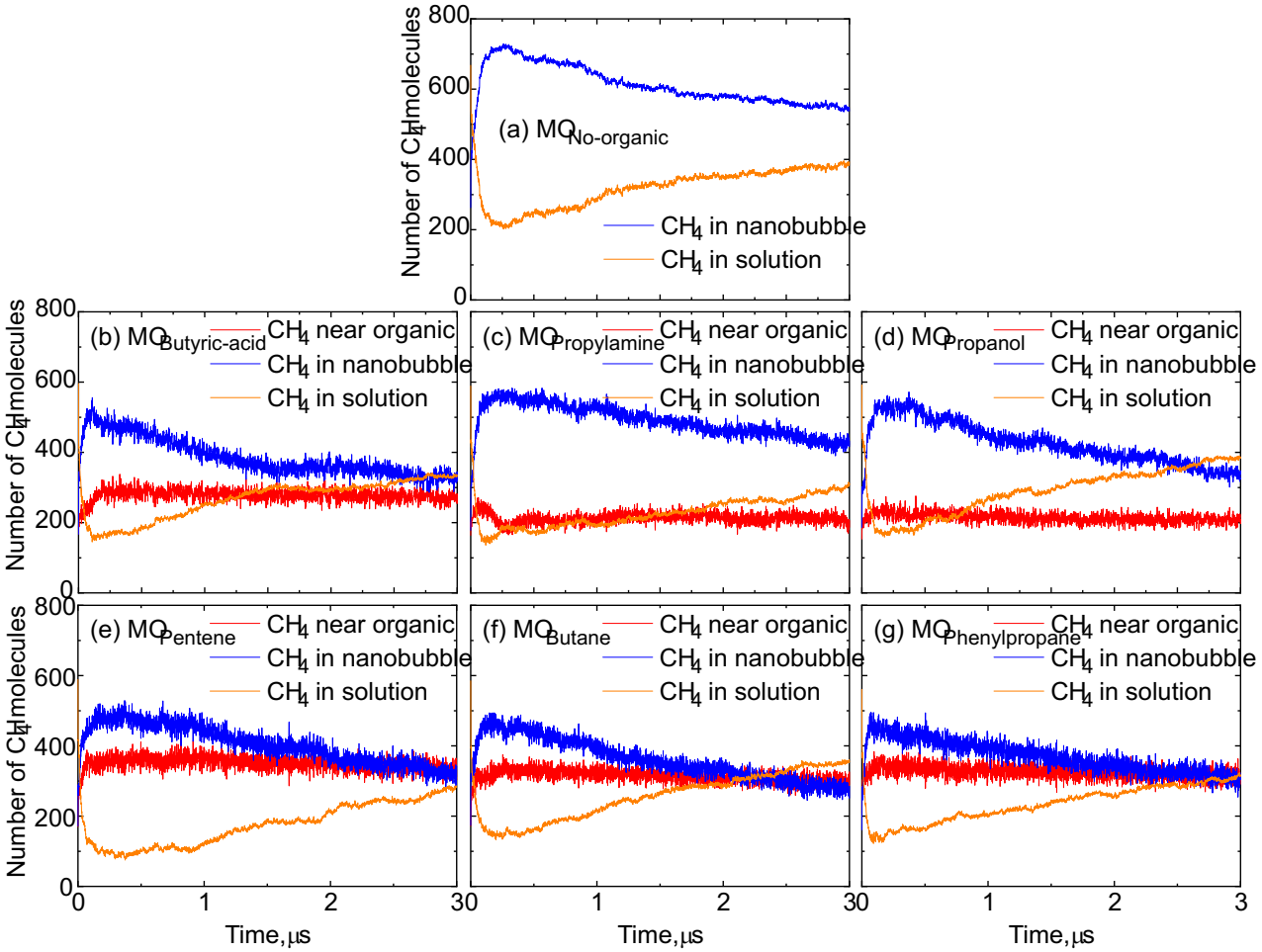


Fig. S11. Evolution of the number of CH_4 in nanobubble, dissolved solution and near the organic molecules in the seven systems *i.e.,* **(a)** $MO_{No\text{-}organic}$, **(b)** $MO_{Butyric\text{-}acid}$, **(c)** $MO_{Propylamine}$, **(d)** $MO_{Propanol}$, **(e)** $MO_{Pentene}$, **(f)** MO_{Butane} and **(g)** $MO_{Phenylpropane}$.

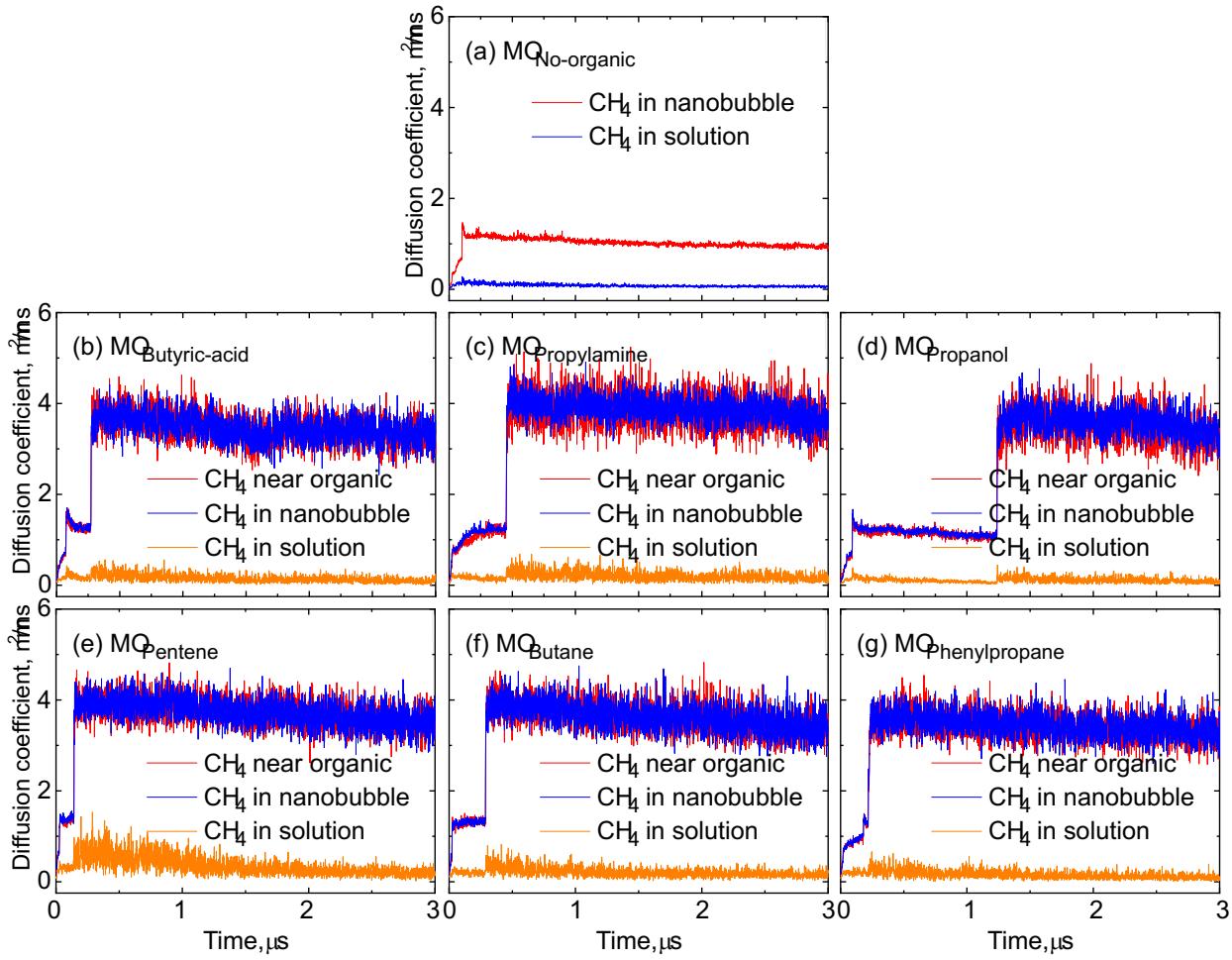


Fig. S12. Evolution of the diffusion coefficient (k_{DC}) for three types of CH_4 molecules during the hydrate formation in the seven systems *i.e.,* **(a)** $MO_{No\text{-}organic}$, **(b)** $MO_{Butyric\text{-}acid}$, **(c)** $MO_{Propylamine}$, **(d)** $MO_{Propanol}$, **(e)** $MO_{Pentene}$, **(f)** MO_{Butane} and **(g)** $MO_{Phenylpropane}$.

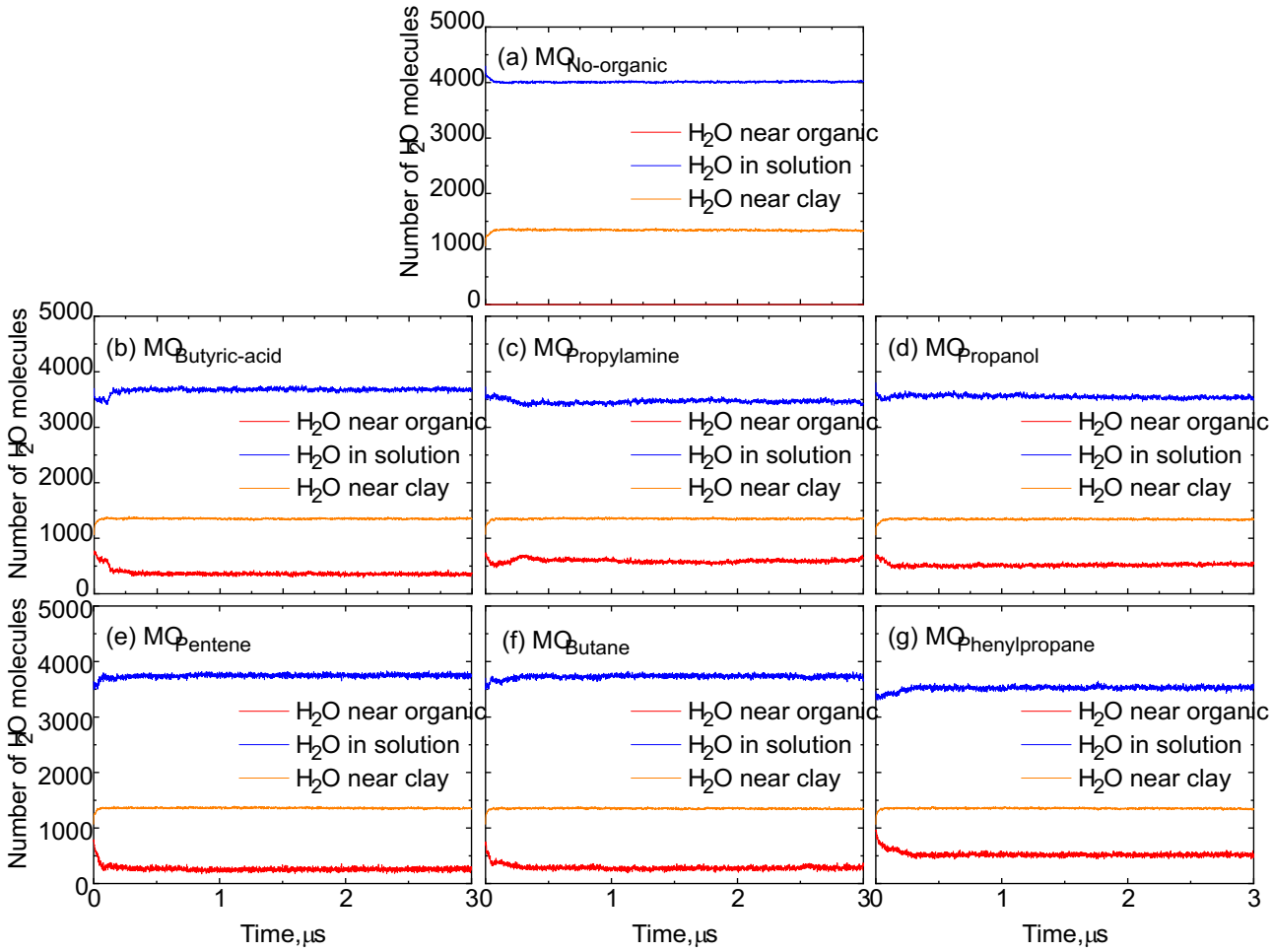


Fig. S13. Evolution of the number of three types of H_2O molecules in the seven systems *i.e.,* **(a)** $MO_{No\text{-}organic}$, **(b)** $MO_{Butyric\text{-}acid}$, **(c)** $MO_{Propylamine}$, **(d)** $MO_{Propanol}$, **(e)** $MO_{Pentene}$, **(f)** MO_{Butane} and **(g)** $MO_{Phenylpropane}$.

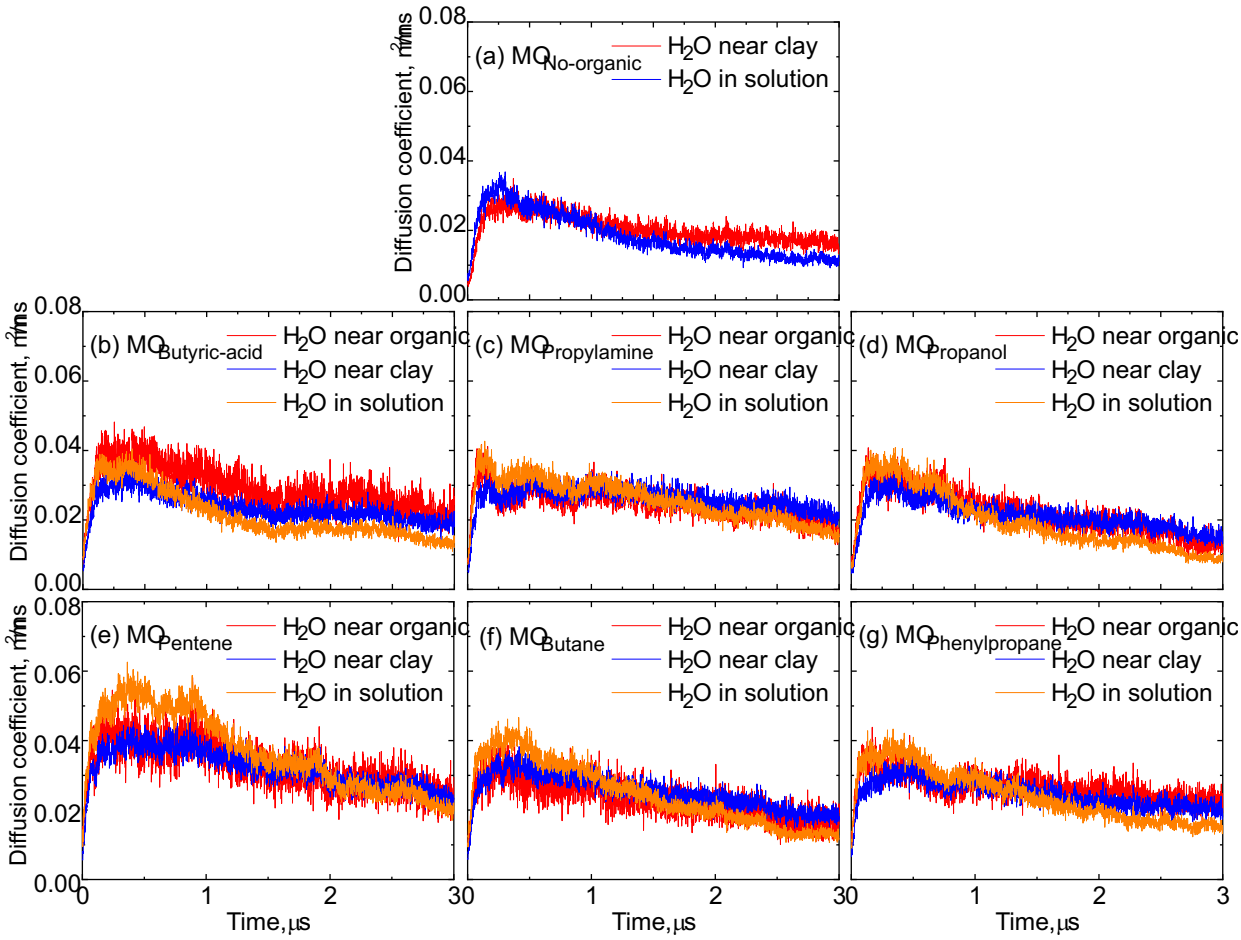


Fig. S14. Evolution of the diffusion coefficient (k_{DC}) for three types of H_2O molecules during the hydrate formation in the seven systems *i.e.,* **(a)** $MO_{No\text{-}organic}$, **(b)** $MO_{Butyric\text{-}acid}$, **(c)** $MO_{Propylamine}$, **(d)** $MO_{Propanol}$, **(e)** $MO_{Pentene}$, **(f)** MO_{Butane} and **(g)** $MO_{Phenylpropane}$.

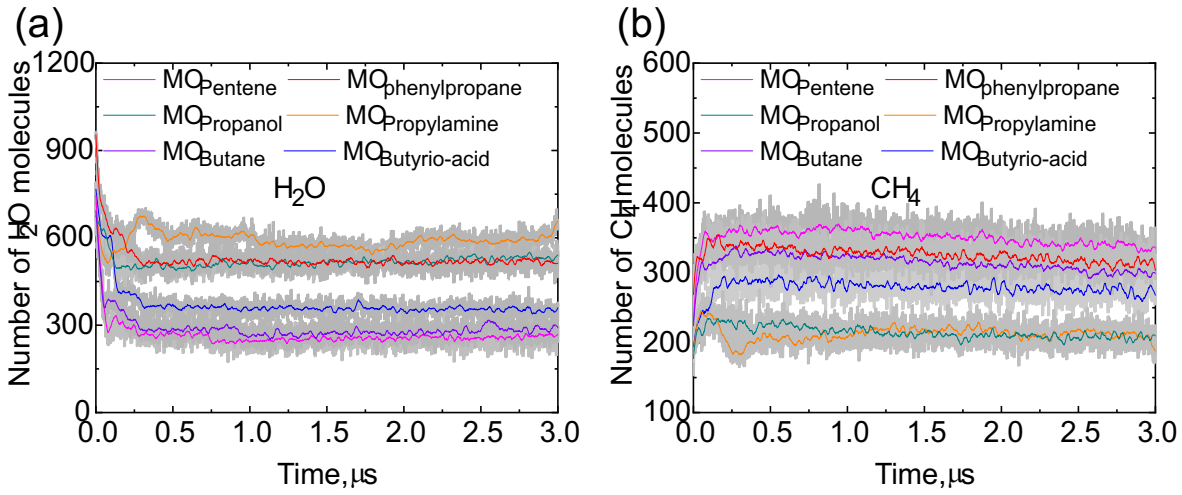


Fig. S15. Evolution of the number of **(a)** H_2O and **(b)** CH_4 molecules near organic molecules in the six systems *i.e.,* $MO_{Butyric\text{-}acid}$, $MO_{Propylamine}$, $MO_{Propanol}$, $MO_{Pentene}$, MO_{Butane} and $MO_{Phenylpropane}$.

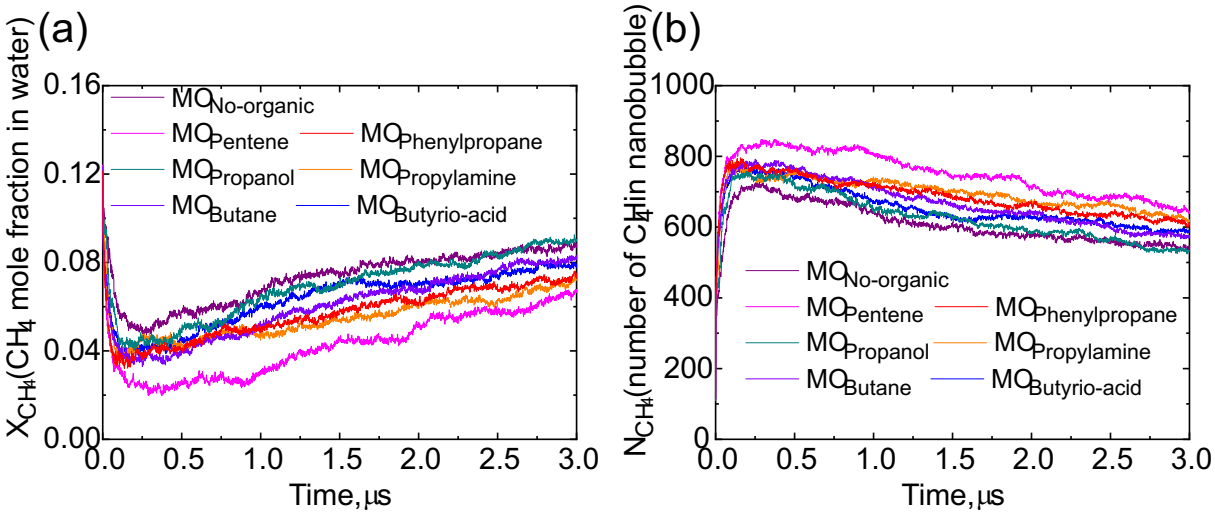


Fig. S16. Evolution of **(a)** CH_4 mole fraction in water (x_{CH4}) for solutions and **(b)** the number of CH_4 molecules in the nanobubbles (N_{CH4}) for the seven systems, *i.e.,* $MO_{No\text{-}organic}$, $MO_{Butyric\text{-}acid}$, $MO_{Propylamine}$, $MO_{Propanol}$, $MO_{Pentene}$, MO_{Butane} and $MO_{Phenylpropane}$.

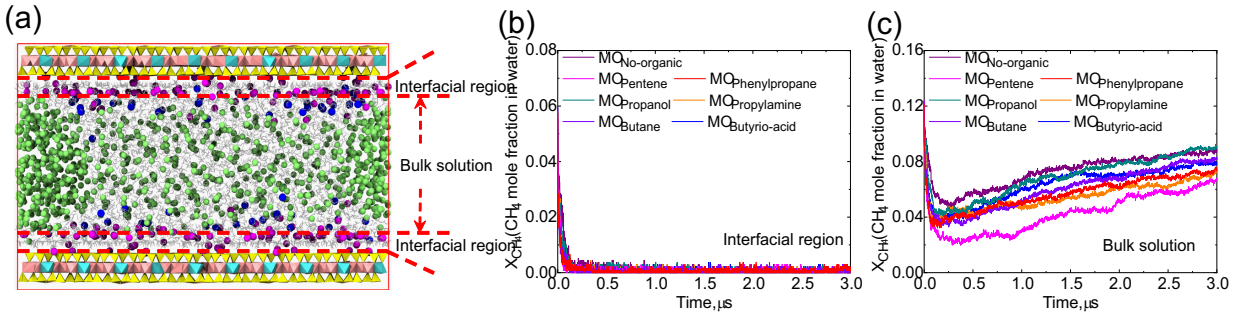


Fig. S17. (a) Schematic representation of the interface region and bulk solution in the simulation box. Evolution of CH_4 mole fraction in water (x_{CH4}) for **(b)** interfacial region and **(c)** bulk solution in the seven systems, *i.e.,* $MO_{No\text{-}organic}$, $MO_{Butyric\text{-}acid}$, $MO_{Propylamine}$, $MO_{Propanol}$, $MO_{Pentene}$, MO_{Butane}, and $MO_{Phenylpropane}$.

Spontaneous nucleation of CH_4 hydrates occurs in the middle region of the nanopores, *i.e.,* the bulk region. At the beginning of the simulation, CH_4 molecules will be separated from the clay surface by the interfacial water layer and the interfacial ion layer, causing the CH_4 concentration in the interface region to drop sharply and unable to provide a gas source for the spontaneous nucleation of CH_4 hydrates (Fig. S17(a)–(b)). At the same time, the large number of salt ions in the interface region will greatly inhibit the spontaneous nucleation of CH_4 hydrate (Fig. S17(a)). Therefore, spontaneous nucleation of CH_4 hydrate does not occur in the interfacial region. For the bulk region, CH_4 molecules in the interface region will quickly move to the bulk region, which increases the CH_4

concentration in the bulk region and is conducive to the spontaneous nucleation of CH_4 hydrate (Fig. S17(c)).

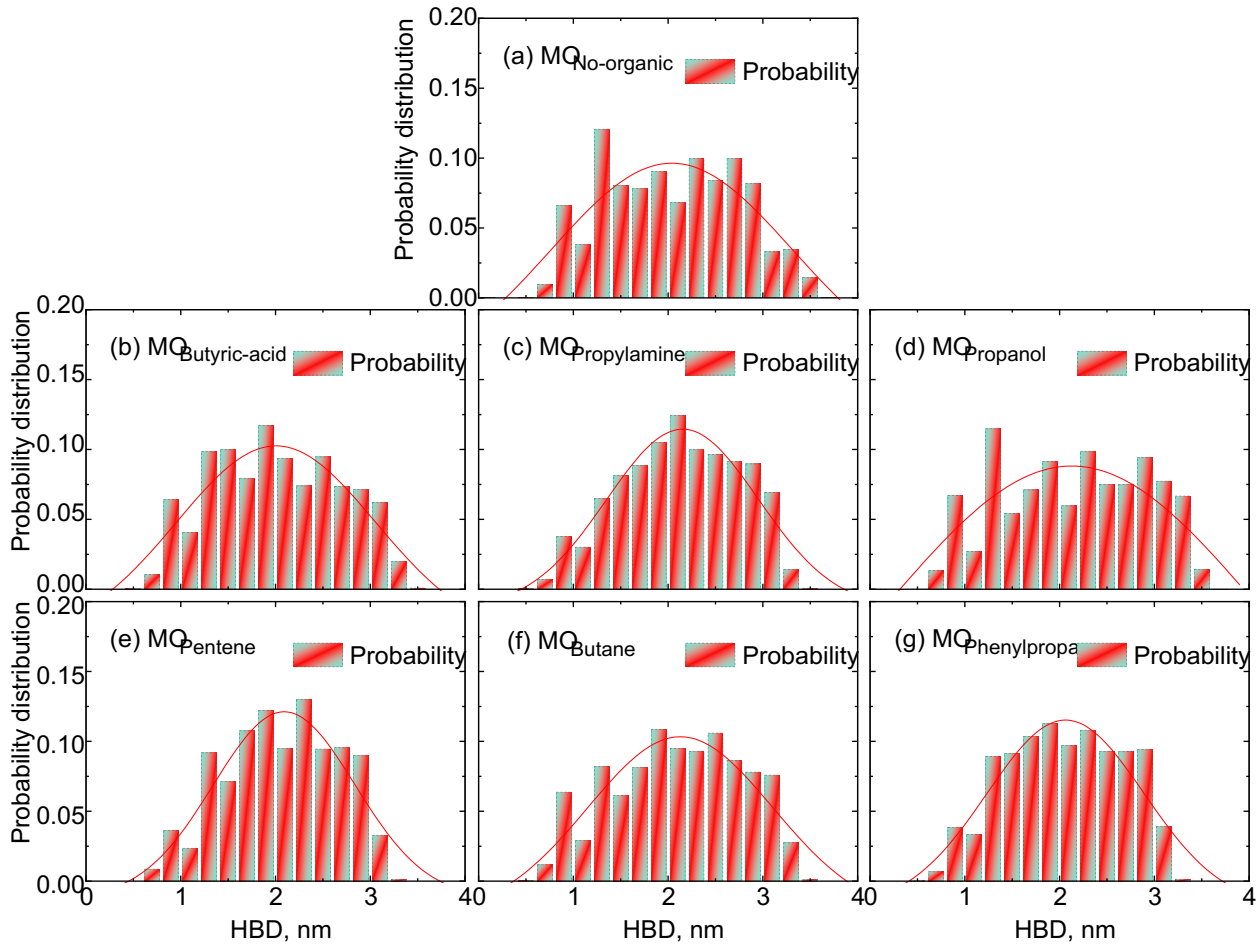


Fig. S18. Probability distribution of the distance between CH_4 in hydrate and nanobubbles (HBD) over the last 0.05 μs in the seven systems *i.e.,* **(a)** $MO_{No\text{-}organic}$, **(b)** $MO_{Butyric\text{-}acid}$, **(c)** $MO_{Propylamine}$, **(d)** $MO_{Propanol}$, **(e)** $MO_{Pentene}$, **(f)** MO_{Butane} and **(g)** $MO_{Phenylpropane}$.

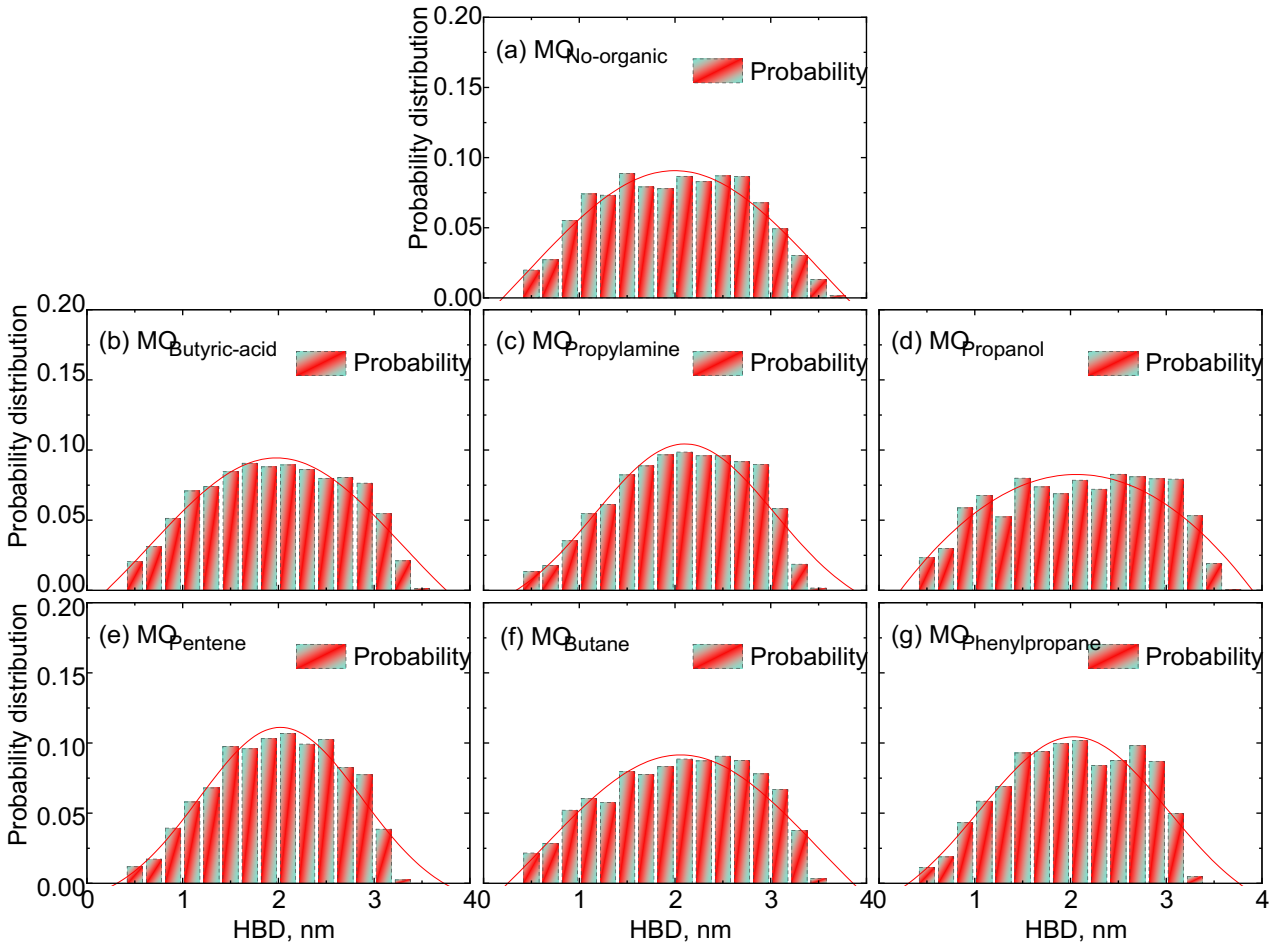


Fig. S19. Probability distribution of the distance between H_2O in hydrate and nanobubbles (HBD) over the last 0.05 μs in the seven systems *i.e.,* **(a)** $MO_{No\text{-}organic}$, **(b)** $MO_{Butyric\text{-}acid}$, **(c)** $MO_{Propylamine}$, **(d)** $MO_{Propanol}$, **(e)** $MO_{Pentene}$, **(f)** MO_{Butane} and **(g)** $MO_{Phenylpropane}$.

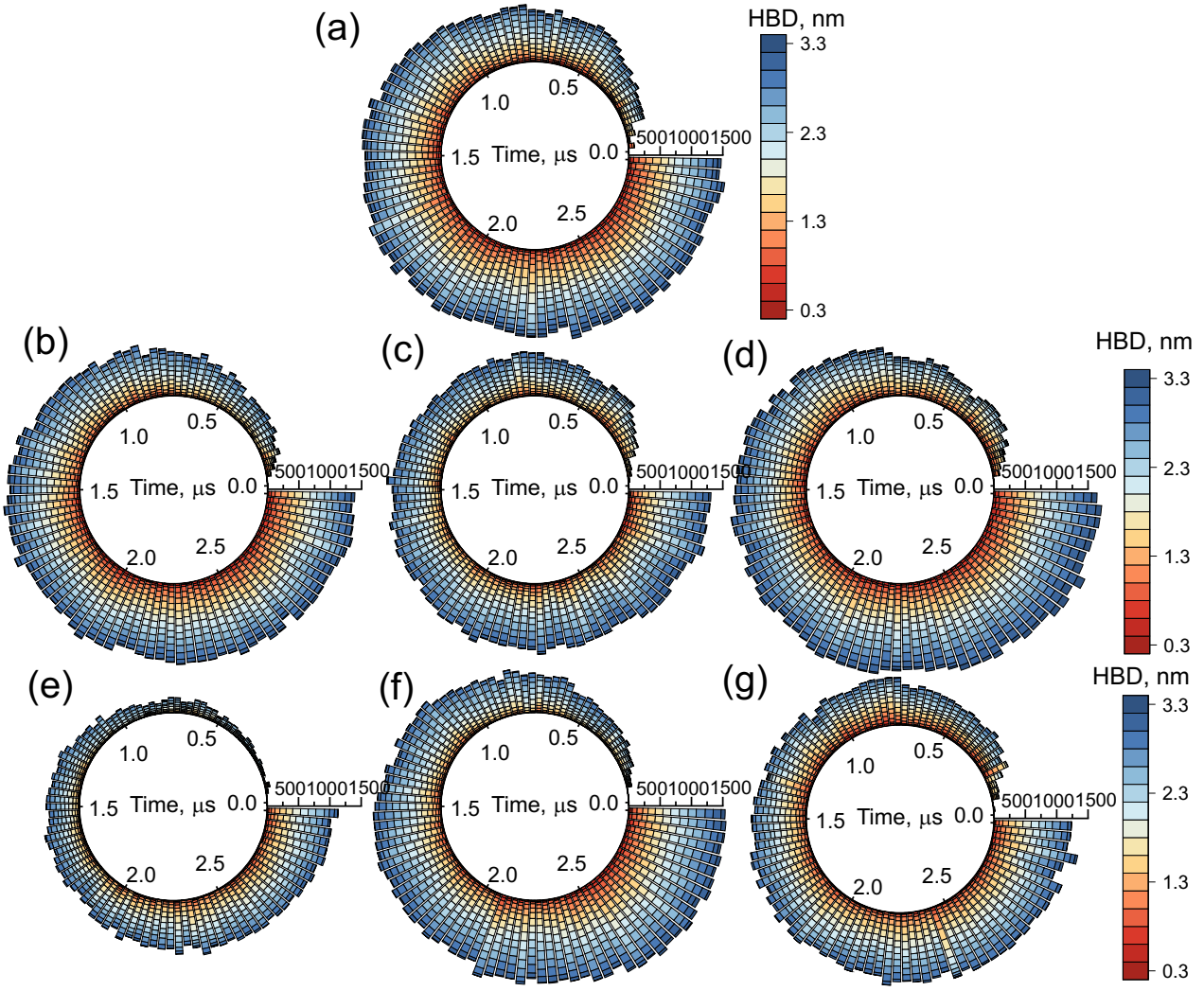


Fig. S20. Evolution of the number of CH_4 molecules in hydrate cages under the distance between hydrate and nanobubbles (HBD) in the seven systems *i.e.,* **(a)** $MO_{No\text{-}organic}$, **(b)** $MO_{Butyric\text{-}acid}$, **(c)** $MO_{Propylamine}$, **(d)** $MO_{Propanol}$, **(e)** $MO_{Pentene}$, **(f)** MO_{Butane} and **(g)** $MO_{Phenylpropane}$.

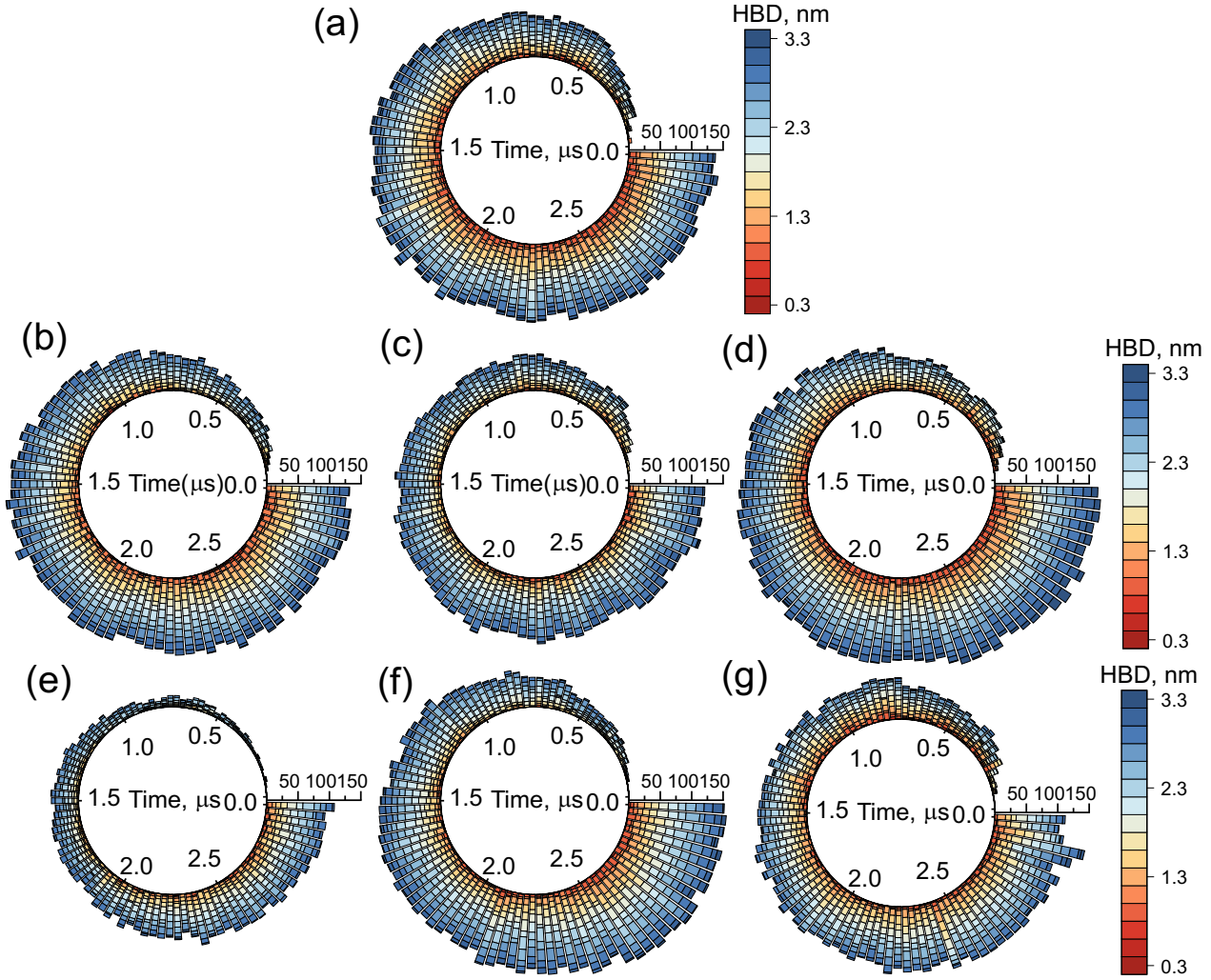


Fig. S21. Evolution of the number of H_2O molecules in hydrate cages under the distance between hydrate and nanobubbles (HBD) in the seven systems *i.e.,* **(a)** $MO_{No\text{-}organic}$, **(b)** $MO_{Butyric\text{-}acid}$, **(c)** $MO_{Propylamine}$, **(d)** $MO_{Propanol}$, **(e)** $MO_{Pentene}$, **(f)** MO_{Butane} and **(g)** $MO_{Phenylpropane}$.

We only select the HBD range 0 - 3.3 nm because only very few CH_4 hydrates spontaneously nucleate in the region beyond 3.3 nm from the CH_4 nanobubbles. The number of CH_4 and H_2O molecules in the hydrate is calculated every 30 ns. It is found that in the $MO_{Propanol}$ system, a large number of CH_4 hydrate can spontaneously nucleate in the region close to the nanobubbles in the early stages of the simulation. This finding also confirms that propanol molecules promote the spontaneous nucleation of CH_4 hydrate from organoclay salt solutions.

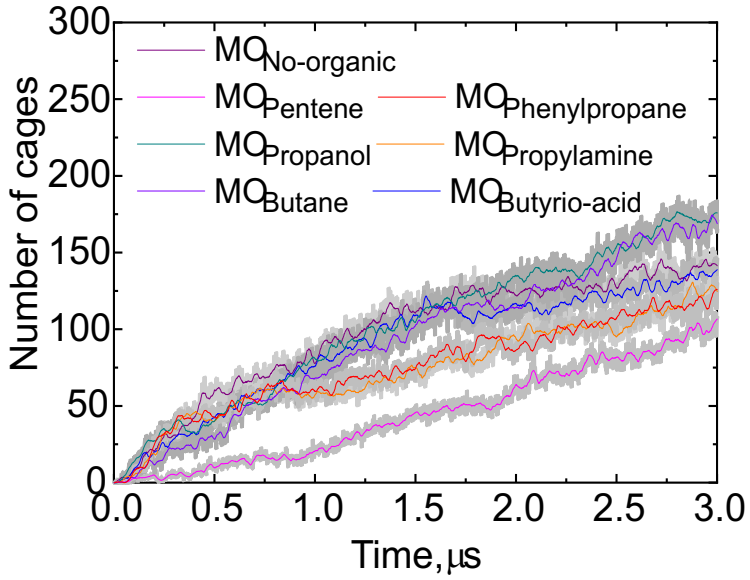


Fig. S22. Evolution of the number of hydrate cages for the seven systems, *i.e.,* $MO_{No\text{-}organic}$, $MO_{Butyric\text{-}acid}$, $MO_{Propylamine}$, $MO_{Propanol}$, $MO_{Pentene}$, MO_{Butane} and $MO_{Phenylpropane}$.

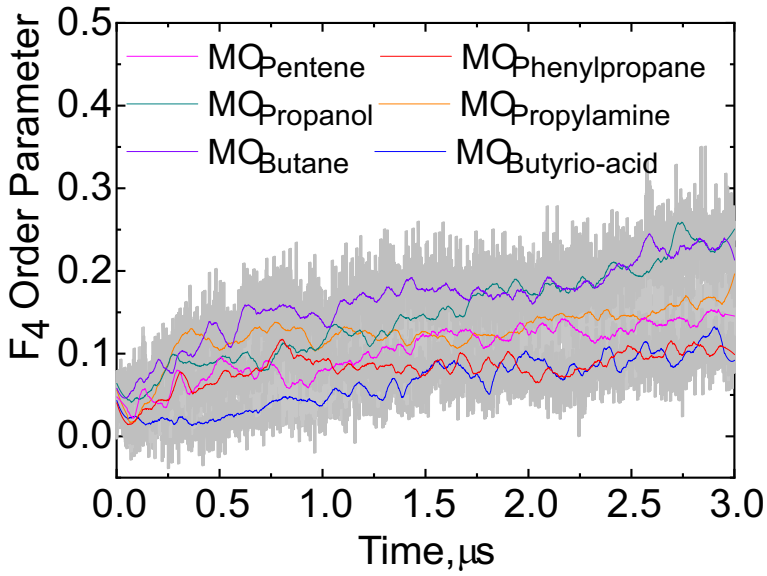


Fig. S23. Evolution of F_4 near the organic molecules in the six systems *i.e.,* $MO_{Butyric\text{-}acid}$, $MO_{Propylamine}$, $MO_{Propanol}$, $MO_{Pentene}$, MO_{Butane} and $MO_{Phenylpropane}$.

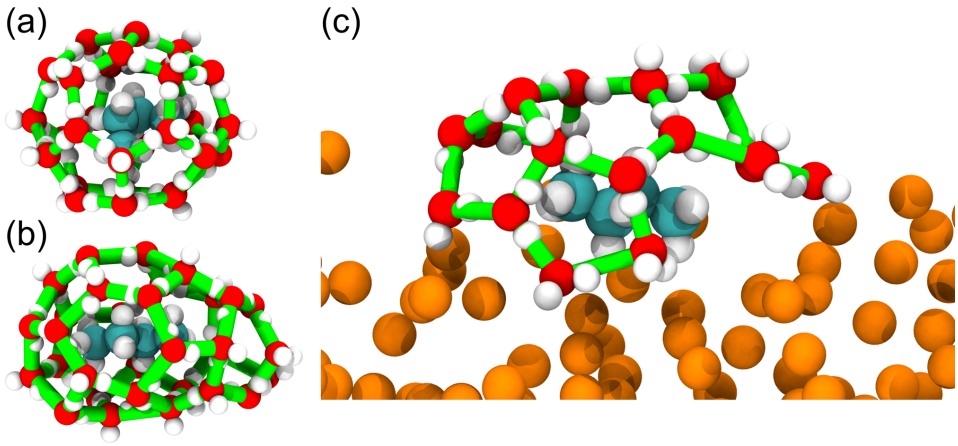


Fig. S24. Snapshots of the **(a)** complete cage and **(b)** cage-like hydrogen-bond networks of water molecules near the butane molecule in the MO_{Butane} system. **(c)** Snapshots of cage-like structures on the surface of butane adsorbed on nanobubble surface.

Butane hydrate is a SII-type hydrate. It is observed that the butane hydrate cages are all of the larger sizes (Fig. S24(a)–(b)). Notably, butane molecules are found to be wrapped between the cage-like hydrogen-bond networks of water molecules and the mixed nanobubbles (Fig. S24(c)), indicating that the water molecules surrounding the butane molecules form a cage-like hydrogen-bond network. This phenomenon may indicate that butane molecules promote the directional arrangement of water molecules around the mixed nanobubbles, thereby promoting the formation of hydrate structures. This may be one of the reasons why butane/CH_4 mixed hydrates form more easily than pure CH_4 hydrates. This finding also provides insights into the formation mechanism of mixed hydrates and is worthy of further exploration.

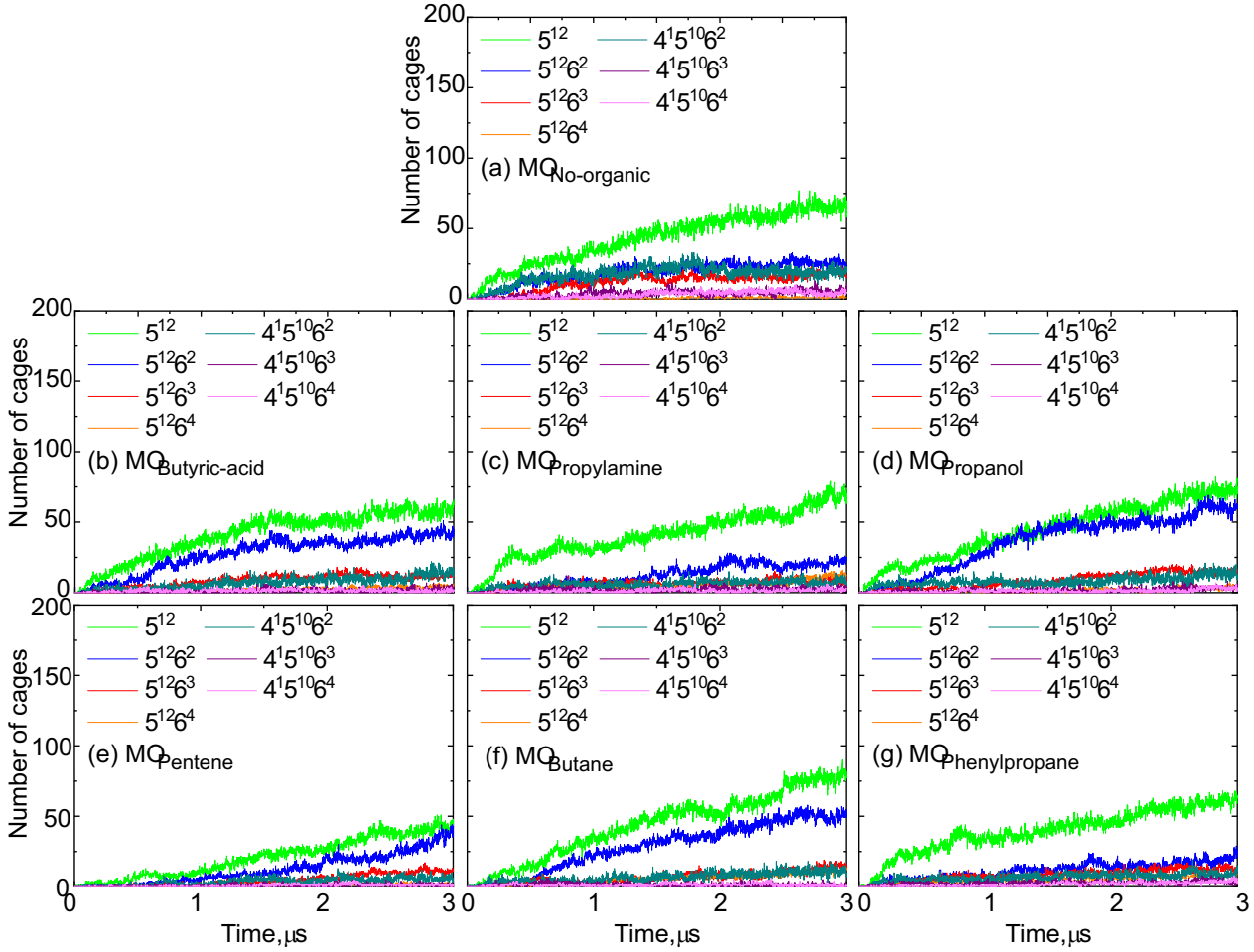


Fig. S25. Evolution of the number of hydrate cages in the seven systems *i.e.,* **(a)** $MO_{No\text{-}organic}$, **(b)** $MO_{Butyric\text{-}acid}$, **(c)** $MO_{Propylamine}$, **(d)** $MO_{Propanol}$, **(e)** $MO_{Pentene}$, **(f)** MO_{Butane} and **(g)** $MO_{Phenylpropane}$.

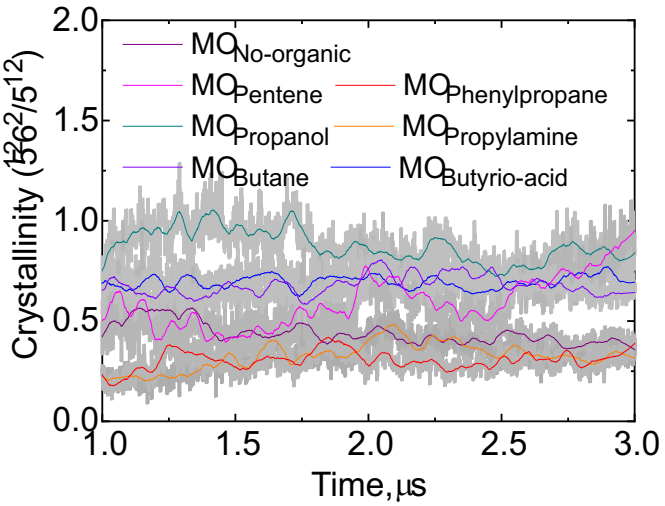


Fig. S26. Evolution of crystallinity ($5^{12}6^2/5^{12}$) for the seven systems, *i.e.,* $MO_{No\text{-}organic}$, $MO_{Butyric\text{-}acid}$, $MO_{Propylamine}$, $MO_{Propanol}$, $MO_{Pentene}$, MO_{Butane} and $MO_{Phenylpropane}$.

S4. Supporting Videos

Video S1. Spontaneous nucleation processes of CH_4 hydrates in the $MO_{No\text{-}organic}$ system. The colored atoms of magnesium (cyan), silicon (yellow), oxygen (red), hydrogen (white), and aluminum (pink) represent the montmorillonite layer. Blue and magenta balls represent Cl^- and Na^+, respectively. Green balls represent CH_4 molecules. Hydrate cages are shown as sticks in various colors (green for 5^{12}, blue for $5^{12}6^2$, red for $5^{12}6^3$, orange for $5^{12}6^4$, cyan for $4^15^{10}6^2$, purple for $4^15^{10}6^3$ and pink for $4^15^{10}6^4$).

Video S2. Spontaneous nucleation processes of CH_4 hydrates in the $MO_{Butyric\text{-}acid}$ system. Butyric-acid molecules are displayed as cyan (C atom), red (O atom) and white (H atom). The colored atoms of magnesium (cyan), silicon (yellow), oxygen (red), hydrogen (white), and aluminum (pink) represent the montmorillonite layer. Blue and magenta balls represent Cl^- and Na^+, respectively. Green balls represent CH_4 molecules. Hydrate cages are shown as sticks in various colors (green for 5^{12}, blue for $5^{12}6^2$, red for $5^{12}6^3$, orange for $5^{12}6^4$, cyan for $4^15^{10}6^2$, purple for $4^15^{10}6^3$ and pink for $4^15^{10}6^4$).

Video S3. Spontaneous nucleation processes of CH_4 hydrates in the $MO_{Propylamine}$ system. Propylamine molecules are displayed as cyan (C atom), blue (N atom) and white (H atom). The colored atoms of magnesium (cyan), silicon (yellow), oxygen (red), hydrogen (white), and aluminum (pink) represent the montmorillonite layer. Blue and magenta balls represent Cl^- and Na^+, respectively. Green balls represent CH_4 molecules. Hydrate cages are shown as sticks in various colors (green for 5^{12}, blue for $5^{12}6^2$, red for $5^{12}6^3$, orange for $5^{12}6^4$, cyan for $4^15^{10}6^2$, purple for $4^15^{10}6^3$ and pink for $4^15^{10}6^4$).

Video S4. Spontaneous nucleation processes of CH_4 hydrates in the $MO_{Propanol}$ system. Propanol molecules are displayed as cyan (C atom), red (O atom) and white (H atom). The colored atoms of magnesium (cyan), silicon (yellow), oxygen (red), hydrogen (white), and aluminum (pink) represent the montmorillonite layer. Blue and magenta balls represent Cl^- and Na^+, respectively. Green balls represent CH_4 molecules. Hydrate cages are shown as sticks in various colors (green for 5^{12}, blue for $5^{12}6^2$, red for $5^{12}6^3$, orange for $5^{12}6^4$, cyan for $4^15^{10}6^2$, purple for $4^15^{10}6^3$ and pink for $4^15^{10}6^4$).

Video S5. Spontaneous nucleation processes of CH_4 hydrates in the $MO_{Pentene}$ system. Pentene molecules are displayed as cyan (C atom) and white (H atom). The colored atoms of magnesium (cyan), silicon (yellow), oxygen (red), hydrogen (white), and aluminum (pink) represent the montmorillonite layer. Blue and magenta balls represent Cl^- and Na^+, respectively. Green balls represent CH_4 molecules. Hydrate cages are shown as sticks in various colors

(green for 5^{12}, blue for $5^{12}6^2$, red for $5^{12}6^3$, orange for $5^{12}6^4$, cyan for $4^15^{10}6^2$, purple for $4^15^{10}6^3$ and pink for $4^15^{10}6^4$).

Video S6. Spontaneous nucleation processes of CH_4 hydrates in the MO_{Butane} system. Butane molecules are displayed as cyan (C atom) and white (H atom). The colored atoms of magnesium (cyan), silicon (yellow), oxygen (red), hydrogen (white), and aluminum (pink) represent the montmorillonite layer. Blue and magenta balls represent Cl^- and Na^+, respectively. Green balls represent CH_4 molecules. Hydrate cages are shown as sticks in various colors (green for 5^{12}, blue for $5^{12}6^2$, red for $5^{12}6^3$, orange for $5^{12}6^4$, cyan for $4^15^{10}6^2$, purple for $4^15^{10}6^3$ and pink for $4^15^{10}6^4$).

Video S7. Spontaneous nucleation processes of CH_4 hydrates in the $MO_{Phenylpropane}$ system. Phenylpropane molecules are displayed as cyan (C atom) and white (H atom). The colored atoms of magnesium (cyan), silicon (yellow), oxygen (red), hydrogen (white), and aluminum (pink) represent the montmorillonite layer. Blue and magenta balls represent Cl^- and Na^+, respectively. Green balls represent CH_4 molecules. Hydrate cages are shown as sticks in various colors (green for 5^{12}, blue for $5^{12}6^2$, red for $5^{12}6^3$, orange for $5^{12}6^4$, cyan for $4^15^{10}6^2$, purple for $4^15^{10}6^3$ and pink for $4^15^{10}6^4$).

Reference

Abascal, J.L., Sanz, E., Garcia Fernandez, R., Vega, C., 2005. A potential model for the study of ices and amorphous water: TIP4P/Ice. J. Chem. Phys. 122, 234511.

Báez, L.A., Clancy, P., 1994. Computer Simulation of the Crystal Growth and Dissolution of Natural Gas Hydrates a. Ann. N.Y. Acad. Sci. 715, 177-186.

Berendsen, H.J.C., Postma, J.P.M., Vangunsteren, W.F., Dinola, A., Haak, J.R., 1984. Molecular dynamics with coupling to an external bath. J. Chem. Phys. 81, 3684-3690.

Bussi, G., Donadio, D., Parrinello, M., 2007. Canonical sampling through velocity rescaling. J. Chem. Phys. 126, 014101.

Cygan, R.T., Liang, J.J., Kalinichev, A.G., 2004. Molecular models of hydroxide, oxyhydroxide, and clay phases and the development of a general force field. J. Phys. Chem. B 108, 1255-1266.

Downs, R.T., Hall-Wallace, M., 2003. The crystal structure database. Am. Mineral. 88, 247-250.

Jacobson, L.C., Hujo, W., Molinero, V., 2009. Thermodynamic stability and growth of guest-free clathrate hydrates: a low-density crystal phase of water. J. Phys. Chem. B 113, 10298-10307.

Jorgensen, W.L., Madura, J.D., Swenson, C.J., 1984. Optimized Intermolecular Potential Functions for Liquid Hydrocarbons. J. Am. Chem. Soc. 106, 6638-6646.

Jorgensen, W.L., Maxwell, D.S., TiradoRives, J., 1996. Development and testing of the OPLS all-atom force field on conformational energetics and properties of organic liquids. J. Am. Chem. Soc. 118, 11225-11236.

Li, Y., Chen, M., Tang, H., Han, S.B., Song, H.Z., Wang, P.F., Zhao, Y.S., Zhu, J.L., 2022. Insights into Carbon Dioxide Hydrate Nucleation on the External Basal Surface of Clay Minerals from Molecular Dynamics Simulations. ACS Sustain. Chem. Eng. 10, 6358-6369.

Loewenstein, W., 1954. The Distribution of Aluminum in the Tetrahedra of Silicates and Aluminates. Am. Mineral. 39, 92-96.

Mi, F., He, Z., Jiang, G., Ning, F., 2022. Effects of marine environments on methane hydrate formation in clay nanopores: A molecular dynamics study. Science of the Total Environment 852, 158454.

Nose, S., 1984. A molecular dynamics method for simulations in the canonical ensemble. Mol. Phys. 52, 255-268.

Parrinello, M., Rahman, A., 1980. Crystal-Structure and Pair Potentials - a Molecular-Dynamics Study. Phys. Rev. Lett. 45, 1196-1199.